Perivascular and parenchymal fluid characteristics are related to age and cognitive performance across the lifespan

Kirsten M. Lynch[1]*, Rachel M. Custer[1], Farshid Sepehrband[1,2], Arthur Toga[1], Jeiran Choupan[1,2]

Affiliations:
[1]Laboratory of Neuro Imaging (LONI), USC Mark and Mary Stevens Institute for Neuroimaging and Informatics, USC Keck School of Medicine, Los Angeles, CA, 90033
[2]NeuroScope Inc., New York, USA

*Corresponding author:
Kirsten M. Lynch
323-442-7246
USC Stevens Neuroimaging and Informatics Institute
Keck School of Medicine of USC
University of Southern California
2025 Zonal Ave.
Los Angeles, CA 90033
Email: kirsten.lynch@loni.usc.edu

Abstract:
Perivascular spaces (PVS) play a critical role in fluid transfer and waste clearance in the brain, but few studies have explored how alterations to perivascular fluid flow may impact brain maturation and behavior. This study aims to characterize age-related alterations to perivascular and parenchymal fluid flow characteristics across the lifespan in typically developing children (8-21 years) and aging adults (35-90 years) and assess their contribution to cognition. In this study, we employ multi-compartment diffusion models, neurite orientation dispersion and density imaging (NODDI) and tissue tensor imaging (TTI), to quantify free water diffusion characteristics within automatically defined perivascular spaces using enhanced PVS contrasts, the surrounding parenchyma, and at variable distances from the PVS. Our findings show free water diffusion characteristics within the PVS and surrounding parenchyma are associated with age and cognitive scores.

Introduction

The waste clearance pathway is the proposed mechanism through which metabolic waste and toxic substrates are removed from the brain. According to the glymphatic hypothesis introduced by Illif and colleagues (Iliff et al., 2013), it is theorized that cerebrospinal fluid (CSF) enters the brain parenchyma via perivascular spaces, mixes with interstitial fluid (ISF) in the brain parenchyma and flushes out metabolic waste via bulk flow via peri-venous spaces. Therefore, efficient fluid flow is critical for the maintenance of proper brain function and homeostasis.

Pathological PVS enlargement is considered a marker of impaired waste clearance (Xue et al., 2020), as enlarged spaces can impede fluid transfer from the PVS to the brain parenchyma. Disruptions in fluid flow can lead to the accumulation of toxic substances, including amyloid beta, thus further exacerbating waste clearance dysfunction (Keable et al., 2016). Previous studies have shown that PVS are pathologically enlarged in a variety of neurodegenerative disorders, including Alzheimer's disease (Banerjee et al., 2017), mild cognitive impairment (Sepehrband et al., 2021), multiple sclerosis (Kilsdonk et al., 2015) and cerebral small vessel disease (CSVD) (Charidimou et al., 2013, 2017; Doubal et al., 2010; Potter et al., 2015). More recently, studies have also shown increased visibility of PVS in structural MRI over the course of the lifespan, where PVS become progressively wider and more numerous with age (Lynch et al., 2023). However, perivascular space morphology alone is likely insufficient to fully describe waste clearance efficiency, as several other factors can inform PVS structure (Okar et al., 2023), including underlying vascular size (Zong et al., 2020), microvessel tortuosity (Sun et al., 2024) and *ex vacuo* atrophy and demyelination (Groeschel et al., 2006; Wardlaw et al., 2013). Therefore, methods sensitized to bulk fluid flow are needed to more comprehensively describe how ISF circulation is altered over the course of healthy aging.

Diffusion-weighted magnetic resonance imaging (DW-MRI) is a non-invasive imaging technique that can provide insight into the molecular movement of water in biological tissue in vivo. DW-MRI is traditionally used to model microstructural features of the brain; however recent studies have shown the diffusion signal is sensitive to fluid flow in the PVS and brain parenchyma (for review, see Barisano et al., 2022). Previous studies in animal models have used diffusion-based MRI sequences to visualize fluid flow along PVS, thus demonstrating the prominent role of vessel pulsatility on fluid movement (Harrison et al., 2018). Additionally, the disruption of fluid transfer between the PVS and parenchyma through inhibition of aquaporin-4 (AQP4) channels are accompanied by alterations in diffusion metrics believed to reflect interstitial fluid stagnation in the brain parenchyma (Debaker et al., 2020; Gomolka et al., 2023). In human studies, researchers have shown altered interstitial fluid behavior in both Alzheimer's disease (Sepehrband, Cabeen, Barisano, et al., 2019; Sepehrband, Cabeen, Choupan, et al., 2019) and CSVD (Jiaerken et al., 2021) in parenchymal tissue, suggestive of waste clearance dysfunction. However, few studies have explored how interstitial fluid dynamics are altered as a consequence of aging and how it may impact cognitive ability in the general population.

Multi-compartment models represent a potentially powerful tool to study fluid flow related to the waste clearance system (Poulain et al., 2023). In the present study, we employ two distinct multi-compartment models, neurite orientation dispersion and density imaging (NODDI) and tissue tensor imaging (TTI), to probe perivascular and interstitial fluid behavior over the course of the lifespan. NODDI is a popular three-compartment model that estimates the intra-cellular, extra-cellular and free water compartments (Zhang et al., 2012). The isotropic volume fraction (fiso) estimates the fraction of a voxel occupied by free, unobstructed diffusion, commonly observed in CSF. TTI is a technique that utilizes a similar approach to free water-eliminated DTI (fwe-DTI), which models the tissue and free water signals as separate tensors (Pasternak et al.,

2009). However, unlike fwe-DTI, TTI capitalizes on the observation that diffusion within PVS have directional preference due to the confines of the astrocytic end feet and models the free water tensor as anisotropic (Sepehrband, Cabeen, Choupan, et al., 2019). Therefore, this technique can distinguish the tissue and free water diffusivities. Together, NODDI and TTI free water measures provide complementary insight into interstitial fluid behavior and can provide important insight into the biophysical processes that give rise to waste clearance alterations in aging.

The goal of this study is to characterize age-related alterations in perivascular and parenchymal fluid flow dynamics using free water diffusion metrics derived from NODDI and TTI over the course of the lifespan. Additionally, we aim to determine whether fluid flow behavior is related to gross cognitive outcomes. We used high-resolution MRI and behavioral data obtained from the Lifespan Human Connectome Projects in Development (n=468, 8-21 years) and Aging (n=507, 35-90 years) to separately explore how fluid dynamics are altered in child development and advancing age. We explored fluid flow properties within automatically segmented PVS and the surrounding parenchyma, as well as how interstitial fluid properties in the brain parenchyma were altered with increasing distance from the PVS to quantify PVS-parenchyma fluid exchange. Lastly, we explore the behavioral implications of altered fluid dynamics by comparing age-related alterations in perivascular and parenchymal diffusion with global cognitive scores.

Methods

Subjects

Data used in this study was acquired through the Lifespan Human Connectome Projects (HCP) in Development (Somerville et al., 2018) and Aging (Bookheimer et al., 2019). The Lifespan HCP in Development (HCP-D) recruited subjects between 5 and 21 years of age from Boston, Los Angeles, Minneapolis, and St. Louis. The Lifespan HCP in Aging (HCP-A) recruited a large sample of subjects over the age of 36 from multiple locations, including Washington University St Louis, University of Minnesota, Massachusetts General Hospital, and the University of California Los Angeles. To focus on typical development and aging across the lifespan, a liberal threshold for inclusionary criteria was applied. Within HCP-D, subjects were excluded if they had neurodevelopmental disorders or were born premature. Additionally, participants with major psychiatric or neurological disorders, stroke, clinical dementia, severe depression that required extensive treatment, macular degeneration and profound hearing loss were excluded from the study. Subjects with impaired cognitive abilities were excluded from the study according to tiered age-appropriate cut-off scores for cognitive tests. Overall, we included 468 subjects (260 F) between 8 and 21 years of age (14.4 $\pm$ 3.8) from HCP-D and 507 subjects (298 F) between 35 and 90 years of age (56.4 $\pm$ 13.7) from HCP-A in the present study, as previously reported in (Lynch et al., 2023).

MRI acquisition

At each of the study locations, subjects were scanned on a Siemens 3T Prisma scanner with an 80 mT gradient coil and a Siemens 32-channel prisma head coil (Harms et al., 2018). T1w MP-RAGE (voxel size=.8 mm isotropic, 4 echoes per line of k-space, FOV = 256 × 240 × 166 mm, matrix = 320 × 300 × 208 slices, 7.7% slice oversampling, GRAPPA = 2, pixel bandwidth = 744 Hz/pixel, TR = 2500 ms, TI = 1000 ms, TE = 1.8/3.6/5.4/7.2 ms, FA = 8 degrees) and T2w turbo spin echo (TSE) scans (voxel size=.8 mm isotropic, 4 echoes per line of k-space, FOV = 256 × 240 × 166 mm, matrix = 320 × 300 × 208 slices, 7.7% slice oversampling, GRAPPA = 2, pixel bandwidth = 744 Hz/pixel, TR = 3200 ms, TE = 564 ms, turbo factor = 314) were used from each subject to delineate the fine PVS structure. Additionally, multi-shell diffusion weighted images (DWI) with 185 diffusion-encoding directions were acquired across 4 consecutive runs

with 28 b=0 s/mm^2 volumes equally interspersed throughout the scans (multi-band factor = 4, voxel size=1.5 mm isotropic, TR=3.23 s, b=1500 and 3000 s/mm^2). Scans were acquired with opposite phase-encoding directions (AP and PA) for distortion correction.

MRI data processing

T1w and T2w structural data were preprocessed with the HCP Preprocessing Pipeline version 4.0.3 (Glasser et al., 2013) using the LONI pipeline (Dinov et al., 2009). These steps include gradient distortion correction, rigid body alignment with boundary-based registration (BBR) (Greve & Fischl, 2009) and brain extraction. Volumes were transformed to MNI space and brought into ACPC alignment. Freesurfer version 6 (http://surfer.nmr.mgh.harvard.edu/) was run on the T1w images to execute motion correction, intensity normalization and automated Talairach transformation (Reuter et al., 2010; Segonne et al., 2004; Sled et al., 1998). Finally, subcortical white matter was segmented from the T1w volume and used as the brain parenchymal mask for subsequent analyses.

dMRI data was preprocessed using the HCP diffusion preprocessing pipeline (Sotiropoulos et al., 2013). Data was corrected for motion, eddy-current distortions and susceptibility-induced artifacts using FSL EDDY (Andersson & Sotiropoulos, 2016). The dMRI data was then denoised using a non-local means filter. The b=0 s/mm^2 volumes were averaged into a single volume and spatially aligned to the T1w and T2w images using a rigid body transformation using ANTs with tricubic interpolation (Avants et al., 2008). The resulting registration was then applied to the dMRI metric volumes to ensure spatial correspondence between the PVS masks and microstructural maps.

Perivascular space segmentation

PVS were visibly enhanced and segmented using an automated image processing approach outlined in (Sepehrband, Barisano, et al., 2019). First, an enhanced PVS contrast (EPC) was generated from the T1w and T2w images. We performed field bias correction and non-local filtering using image self-similarity properties on the T1w and T2w images. To increase PVS visibility, we then divided the filtered images (T1w/T2w). Next, we segmented the PVS from the EPC using thresholded maps. Briefly, PVS vesselness maps were derived from Frangi filters (default values $\alpha = \beta = 0.5$) applied to the EPC (Frangi et al., 1998). The vesselness maps were then thresholded using optimized thresholding (scaled $t = 1.5$) based on the highest concordance and correlation with values derived from expert readers in the HCP Young Adult dataset (Sepehrband, Barisano, et al., 2019). We have recently found that this thresholding value also performs well in the HCP Lifespan dataset (Lynch et al., 2023). PVS labels with less than 3 contiguous voxels were removed from the total brain mask.

Diffusion models

Microstructural diffusion maps were computed using the Quantitative Imaging Toolkit (QIT) (Cabeen et al., 2018). Microstructural metrics indicative of free water diffusion behaviors were derived from the multi-compartment models NODDI and TTI. The isotropic volume fraction (FISO) from the NODDI model (Zhang et al., 2012) was calculated within each voxel using the spherical mean technique implemented with QIT (Cabeen et al., 2019). The NODDI model adopts a three-compartment model that distinguishes intracellular, extracellular and CSF compartments. FISO reflects the CSF compartment and represents the fraction of the voxel occupied by fast, isotropic Gaussian diffusion.

TTI is a multi-compartment extension of DTI. While DTI measures reflect the diffusion properties of both tissue and fluid from parenchymal PVS, TTI models separate tensors for the tissue and non-parenchymal fluid (Sepehrband, Cabeen, Choupan, et al., 2019). TTI measures were first

initialized using parameters derived from the bi-tensor model, free water-eliminated DTI (fwe-DTI), using iterative least squares optimization (Hoy et al., 2014). For the TTI procedure, the fluid compartment was required to be axially symmetric with positive diffusivities and modeled as an aligned zeppelin. The tissue compartment was re-parameterized with the Cholesky decomposition. The free water diffusivity measures axial diffusivity (fAD), radial diffusivity (fRD), mean diffusivity (fMD) and fractional anisotropy (fFA) were extracted from each voxel and used in subsequent analyses (**Figure 1A**).

The NODDI and TTI measures were averaged within the PVS masks for each subject to obtain estimates of perivascular fluid flow. PVS masks were also subtracted from the white matter masks to obtain parenchymal tissue masks without the contribution of perivascular free water. Diffusion measures were then averaged for each subject within the parenchyma masks. Lastly, to assess how parenchymal diffusion measures change with distance from the PVS, we derived 10 equidistant rings originating from the PVS masks spaced 1 mm apart and computed diffusion measures within each ring mask (**Figure 1A**). This resulted in separate ring masks for each of the 10 possible distances from the PVS (1mm surrounding PVS, 2mm from PVS, 3mm from PVS, etc.).

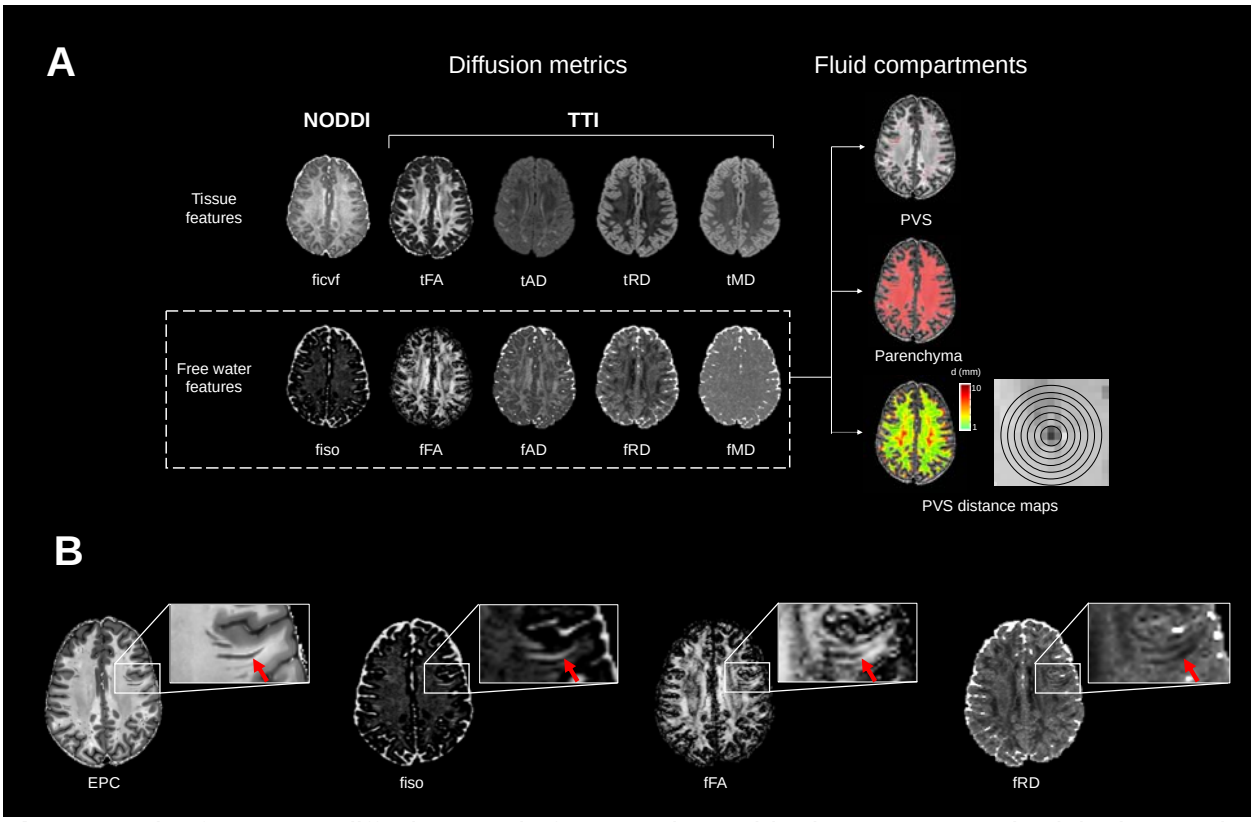

Figure 1. The free water diffusion metric framework used in the present study. (A) The neurite orientation dispersion and density imaging (NODDI) and tissue tensor imaging (TTI) models were run on the diffusion MRI data, yielding the tissue features (ficvf, tFA, tAD, tRD and tMD) and the complementary free water features (fiso, fFA, fAD, fRD and fMD). The free water diffusion features were then averaged within segmented PVS, the PVS-subtracted brain parenchyma, and within 1-mm thick concentric rings surrounding the PVS. (B) The presence of PVS can be observed in an enhanced PVS contrast (EPC) axial slice. These PVS are clearly visible on the same axial slices of fiso, fFA and fRD maps.

Cognitive scores

All subjects in the HCP-D and HCP-A were administered the NIH Toolbox Cognitive Function Battery (Weintraub et al 2013). We used the total cognitive composite scores, which reflected overall cognition determined from both crystallized (ability to recall past learning abilities) and fluid (ability to apply new learning abilities to novel situations) cognitive abilities.

The NIH Toolbox cognitive assessments consist of 7 test instruments that measure 8 abilities within 6 major cognitive domains. The total cognitive composite score combines performance across cognitive domains to yield a composite score indicative of overall, global cognition. Because the present study focuses on the role of free water diffusion within the entire brain across the lifespan, we hypothesize that alterations to waste clearance function would lead to compromises in global cognitive abilities.

Statistical analysis

Effects of Age on Diffusion Measures within Parenchyma and PVS

Diffusion measures were approximately normally distributed within the parenchymal and perivascular masks. Therefore, the main effect of age on mean parenchymal and perivascular free water diffusion measures were assessed with a linear model and we included sex and scan location as covariates of no interest in HCP-D and HCP-A separately.

Effects of Diffusion Measures on Cognition

The role of perivascular and parenchymal free water diffusion processes on cognition throughout the lifespan were assessed using linear models, where we calculated the interaction between total cognition composite scores and age on diffusion metrics separately for HCP-D and HCP-A The choice to analyze HCP-D and HCP-A separately stems from the fact that we had missing data for participants between the ages of 21 and 35 years of age, alongside the notion that cognitive abilities manifest differently in development versus aging.

Effect of Distance from PVS on Diffusion Metrics within Parenchyma

A linear mixed effects (LME) model with maximum likelihood estimation was used to ascertain how parenchymal free water changes with distance from the PVS. LME analysis employs a multilevel modeling approach and considers data collected at various distances from the PVS of each subject as a cluster and thus allows for comparison between rates of change. A random intercept model was employed so that diffusion measures are predicted by the fixed effects including the intercept that varies across subjects. The main effect of distance from PVS on NODDI and TTI measures were assessed. The interaction between cohort (HCP-D and HCP-A) and distance from PVS on diffusion measures were measured.

Results

Free water diffusion measures showed contrast differences between the PVS and parenchyma (**Figure 1B**). Across both cohorts, white matter PVS had significantly higher fiso ($t(974) = 161.61$, $p<.001$), fFA ($t(974) = 106.42$, $p<.001$) and fAD ($t(974) = 57.45$, $p<.001$), and lower fRD ($t(974) = --71.56$, $p<.001$) and fMD ($t(974) = -20.67$, $p<.001$) compared to the surrounding brain parenchyma (**Figure 2**).

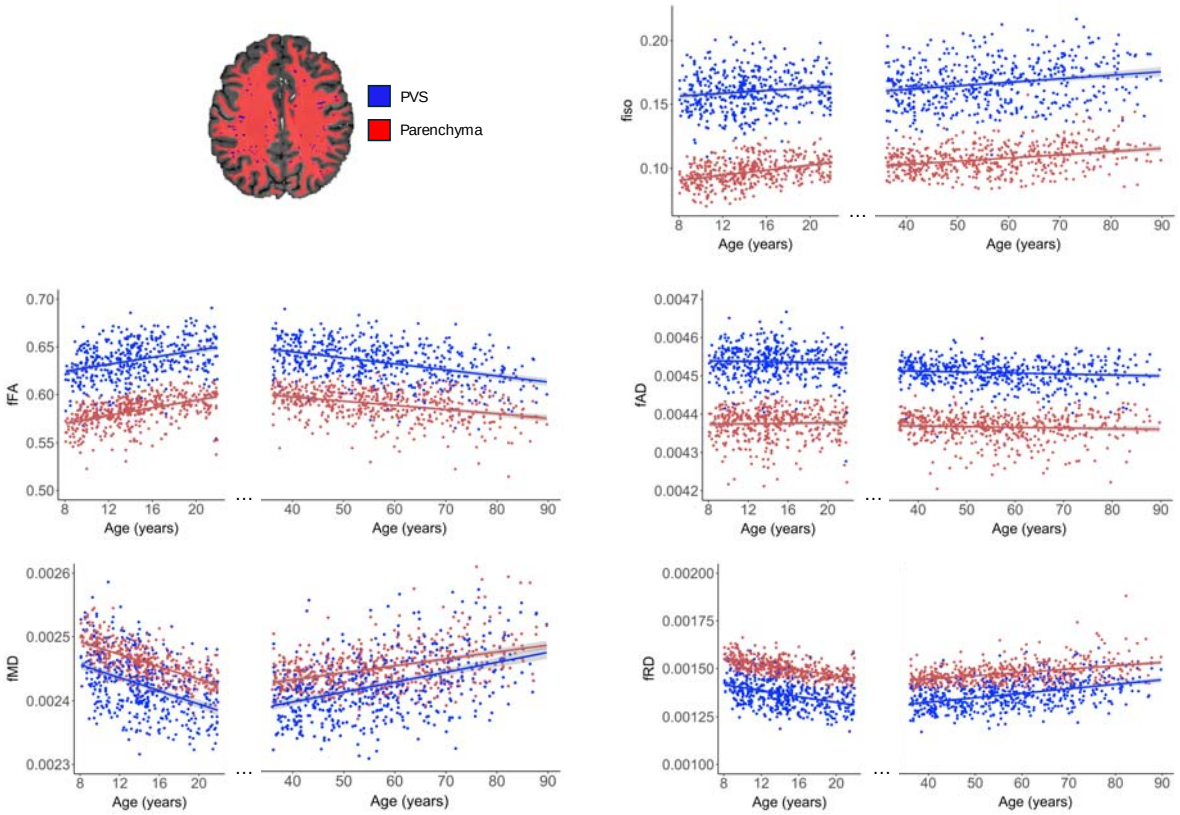

Figure 2. Free water diffusion measures are differentially associated with age across the lifespan. Free water diffusion measures are correlated with age in the developing and aging cohort within the PVS (blue) and brain parenchyma (red).

Age-related alterations in free water diffusion metrics

Within PVS and the surrounding brain parenchyma, fFA increased with age in development and decreased in aging, while fMD and fRD decreased with age in development and increased in aging (**Figure 2**). While ficvf showed rapid increases in development and gradual decline in aging (**Supplementary Figure 1**), fiso increased steadily with age across the lifespan. Because PVS become progressively larger with age (Lynch et al., 2023), we sought to determine whether free water diffusion alterations were due to age-related perivascular dilation. All perivascular free water diffusion measures were significantly associated with the mean diameter of the white matter PVS (**Supplementary Figure 1A**). Within the parenchyma, only fiso was significantly associated with increased PVS diameter (**Supplementary Figure 1B**). The main effect of age on free water tensor metrics remained significant after adjusting for sex and PVS diameter in the model (**Tables 1 and 2**), suggesting that these free water metrics alterations are independent of age-related PVS expansion. Age was not significantly associated with fAD in either cohort.

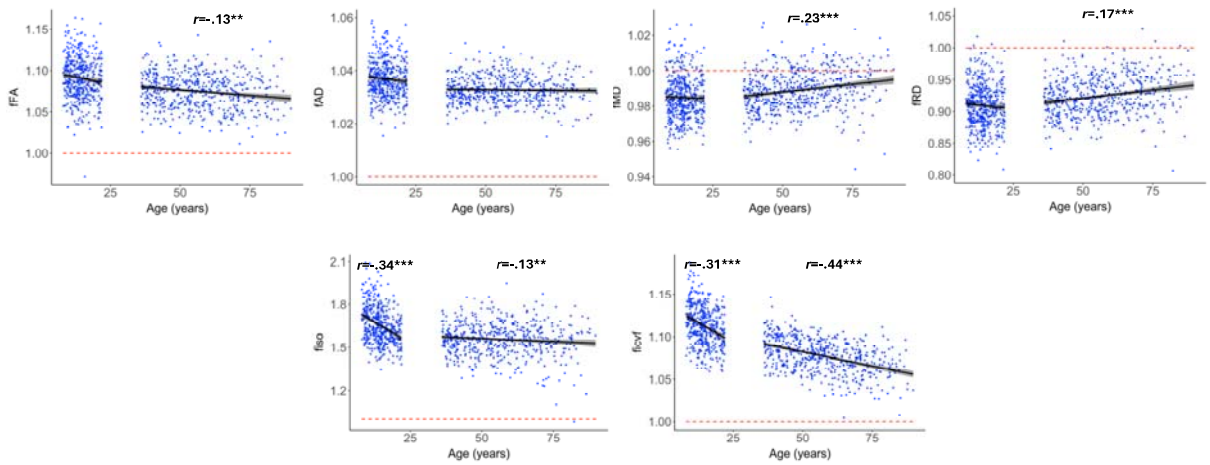

Figure 3. The relationship between age and the ratio between PVS and parenchymal free diffusion. Free water diffusion measures expressed as the ratio between PVS and parenchyma are correlated with age. A value of 1 denotes subjects where the diffusion metric is the same between the PVS and parenchyma (dashed red line). Values greater than one indicate metrics that are higher in the PVS compared to the parenchyma, and values lower than one indicate metrics that are lower in the PVS compared to the parenchyma. Significant correlations with age are indicated where the correlation coefficient (*r*) is shown. * *p*<.05, ** *p*<.01, *** *p*<.001.

The parenchymal and perivascular diffusion metrics had different age-related slopes. To further investigate this interaction, we explored the relationship between age and the ratio between perivascular and parenchymal fluid characteristics. By using this derived measured, perivascular and parenchymal diffusion trends with age can be more directly compared, as values diverging from 1 indicate increased separation in diffusion metrics between perivascular and parenchymal compartments. The ratio between perivascular and parenchymal fMD, fRD, fFA and fiso were significantly associated with age, such that diffusion characteristics in the PVS and surrounding white matter became more similar over time (**Figure 3**). The ratio of fAD in the PVS and parenchyma remains relatively constant across ages.

Age-related alterations to parenchymal free water are dependent on distance from PVS

According to the glymphatic hypothesis, fluid enters the brain parenchyma from the PVS. Therefore, we would expect age-related alterations in free water characteristics at variable distances from the PVS if fluid infiltration is altered in aging. We next sought to characterize how free water diffusion measures in the parenchyma change with distance from the PVS using masks drawn at sequential 1 mm thick concentric rings around the PVS. Using linear mixed effects models, we found that fFA (B=-.014, t(8392)=-347.8, p<.001), fAD (B=-3.4x10^{-5}, t t(8392)=-355.6, p<.001), and fiso (B=-.0089, t t(8392)=-140.8, p<.001) decreased, while fRD (B=4.23x10^{-5}, t t(8392)=141.3, p<.001), and fMD (B=1.48x10^{-5}, t t(8392)=243.7, p<.001) increased with distance from the PVS, indicative of decreased free water in parenchymal regions furthest from the PVS. A significant interaction between cohort and distance from PVS was observed in all free water metrics, where the rate of change in free water diffusion metrics with distance from the PVS was greater in the aging cohort compared to the developing cohort (**Figure 4**).

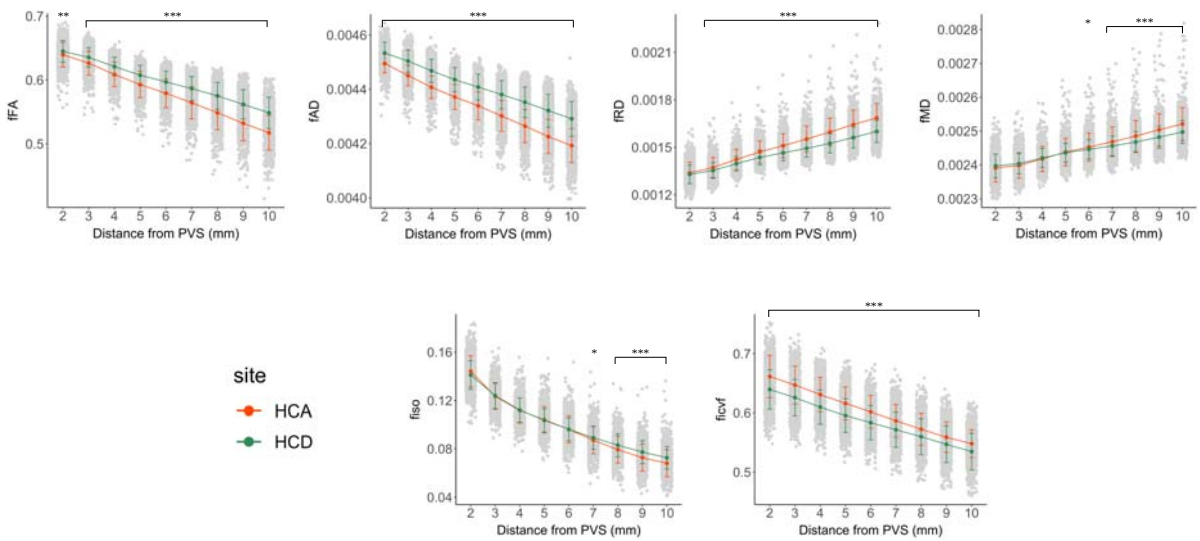

Figure 4. The change in free water diffusion measures with distance from PVS differ with age. Free water diffusion measures were averaged within 1-mm concentric circles emanating from PVS and analyzed in HCP-D (green line) and HCP-A (orange line) separately. Significant differences indicate rings around the PVS where diffusion metrics differ between HCP-A and HCP-D. Significant differences in parenchymal fluid characteristics between developing and aging cohorts were observed across diffusion metrics in regions furthest from the PVS (8-10 mm). T-tests were performed at each discrete distance to assess significant differences in HCP-A and HCP-D. * p<.05, ** p<.01, *** p<.001.

The relationship between free water diffusion measures and cognition is dependent on age

To understand the role perivascular and parenchymal fluid dynamics play in cognitive health across the lifespan, we correlated free water diffusion measures, fFA and fiso, with measures of gross cognitive function using the NIH total cognition composite scores after accounting for age and sex. Within the aging cohort, no significant associations were observed between cognition and fFA in the PVS (t(503)=.442, p=.66) and surrounding parenchyma (t(503)=1.23, p=.22). In the developing cohort, a significant interaction was observed between total cognition and fFA in the PVS (t(464)=-4.09, p=5.0 x 10^{-5}) and parenchyma (t(464)=-3.94, p=9.9 x 10^{-5}), such that the slope is decreased in older adolescents compared to younger children (**Figure 5A and B**).

A. PVS

HCP Development (8-21 years)

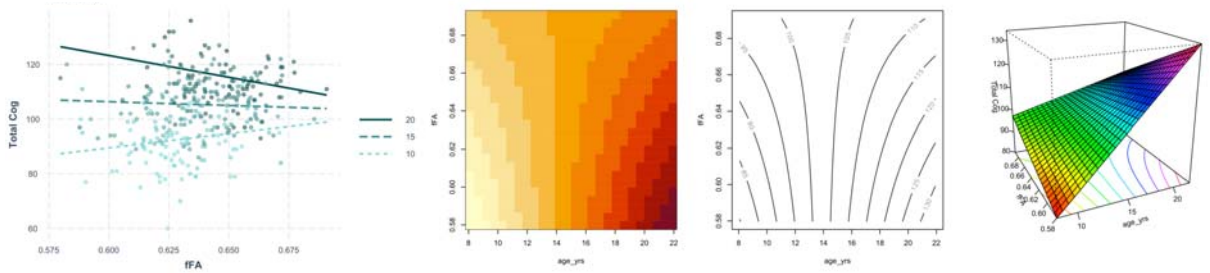

HCP Aging (35-90 years)

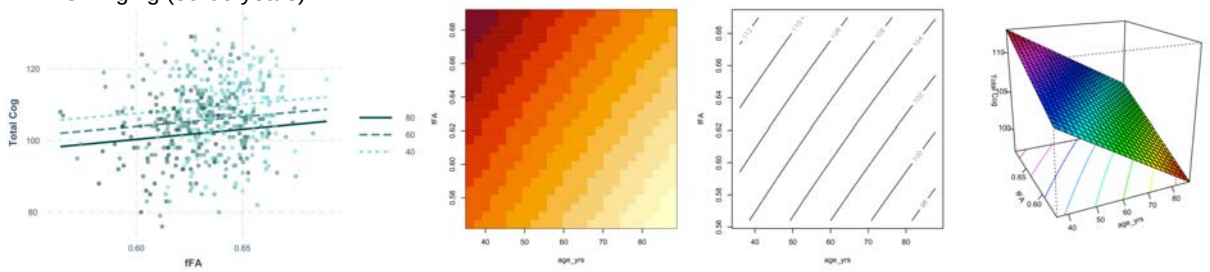

B. Parenchyma

HCP Development (8-21 years)

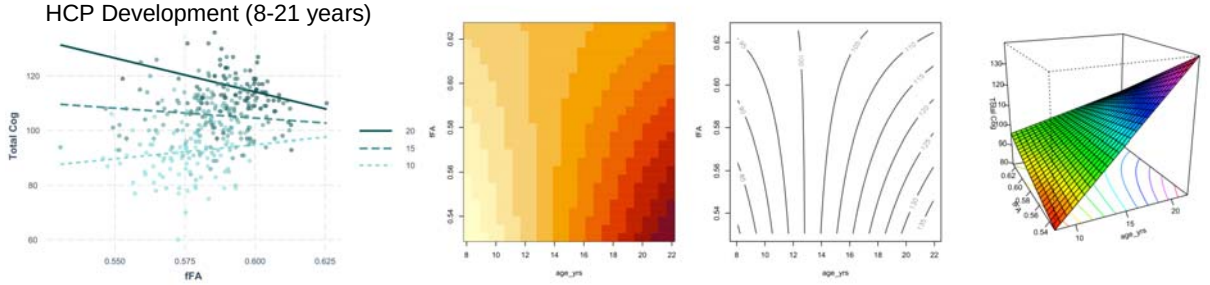

HCP Aging (35-90 years)

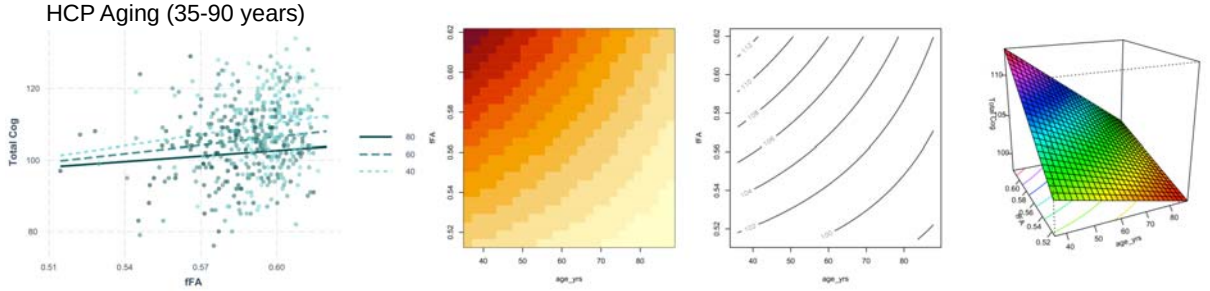

Figure 5. The relationship between free water diffusion and cognition differs across ages. The relationship between fFA and the NIH total cognition composite score (Total Cog) is shown for the (A) PVS and (B) parenchyma. A significant interaction between fFA and age is observed in HCP-D, but not HCP-A. (Left) Individual subjects are shown as points color-coded by age, and representative regression lines are shown for the youngest, middle and oldest ages (from light to dark) for each cohort. (Right) Visualization of the three-dimensional nature of the continuous-by-continuous interactions using matrix plots with contour lines and perspective plots.

When exploring the developing and aging cohorts separately, we found no significant association between total cognition and perivascular and parenchymal fiso in either cohort after controlling for the effects of age and sex (**Table 4; Supplementary Figure 3A and B)**. However, when combining the data together, we found a significant interaction between parenchymal fiso and cohort ($F(974,1)=24.89$, $p=7.5 \times 10^{-7}$), such that increased fiso trends towards greater cognitive outcomes in the developing cohort ($t(466)=1.69$, $p=.09$) and towards worse cognitive outcomes in the aging cohort (t(505)=-1.92, p=.05) after adjusting for subject age (**Supplementary Figure 4A**).

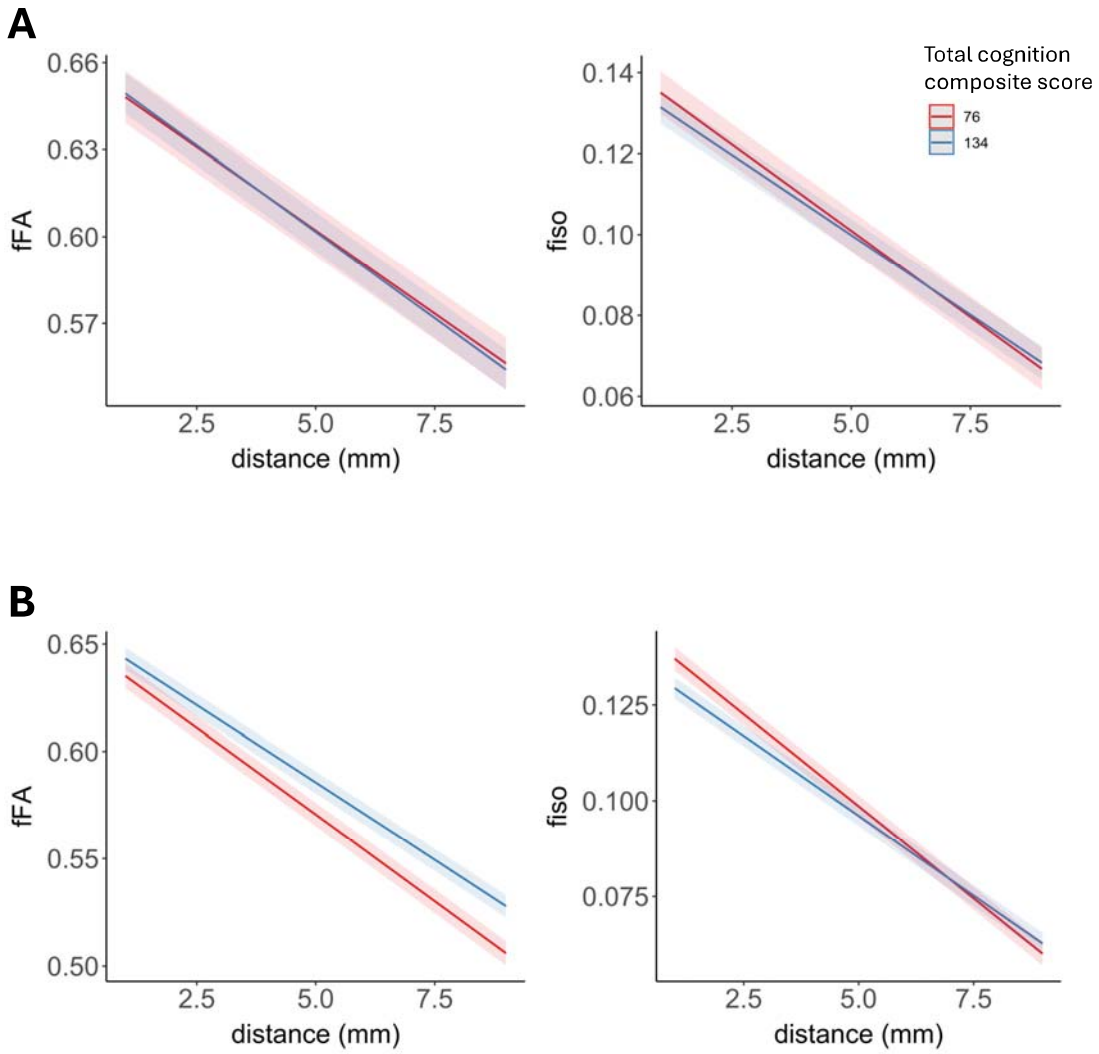

Figure 6. Free water diffusion measures change more rapidly with distance from PVS in subjects with lower cognitive performance. The interaction between NIH Toolbox total cognition composite scores and distance from PVS on parenchymal free water diffusion measures (fFA and fiso) are shown for (A) developing children (8-21 years) and (B) aging adults (35-90 years). The estimated regression lines are derived from linear mixed effects models that account for age and sex in the model. Estimated regression lines are shown for 1 standard deviation below (score of 76) and 1 standard deviation above (score of 136) the mean (score of 100).

Next, we assessed whether diffusivity changes with distance from PVS inform cognition across the lifespan. Using linear mixed effects models, we found fiso varied across distances from PVS according to cognitive performance ($t(2576)=2.39$, $p=.01$), while no significant interaction was observed for fFA ($t(2576)=-1.17$, $p=.24$) in the developing cohort (**Figure 6A**). In the aging cohort, we found a significant interaction between distance from PVS and total cognition scores on fiso ($t(3793)=5.73$, $p=1.1 \times 10^{-8}$) and fFA ($t(3793)=5.74$, $p=9.9 \times 10^{-9}$) after controlling for age and sex (**Figure 6B**). For fiso in all cohorts and fFA in the aging cohort only, free water diffusion measures decrease faster with distance from PVS in subjects with lower cognitive performance (**Figure 6**).

Discussion

In the present study, we used free water diffusion MRI metrics derived from multi-compartment models to assess age-related alterations in perivascular CSF and parenchymal interstitial fluid flow across the lifespan. We found age-related alterations in free water diffusion measures that are distinct from the typical microstructural lifespan trajectories. Additionally, we found age-related differences in parenchymal interstitial fluid content with distance from the PVS, where much sharper drop-offs in fluid content are observed in aging adults compared to development. Lastly, fluid behavior in the parenchyma and PVS differentially predicted cognitive performance across age ranges.

Our findings reiterated previous studies that show perivascular and parenchymal fluid compartments can be visually and statistically separated using free water diffusion maps. Our findings show the free water volume fraction is highest in the PVS, presumably due to the increased content of freely diffusing fluid within the PVS compared to the hindered barriers of the brain parenchyma, replete with axons, glia and metabolic debri in the extracellular space. Additionally, we found free water anisotropy is highest in the PVS compared to the parenchyma. This is likely attributed to the preferential movement of unhindered fluid along the length of the PVS compared to the more tortuous path bulk fluid must take through the brain parenchyma. Previous studies have indeed demonstrated that perivascular fluid systematically biases the traditional DTI signal due to the presence of fast diffusion of CSF within the confines of the PVS (Sepehrband, Cabeen, Choupan, et al., 2019).

Our findings demonstrate that perivascular and parenchymal fiso increase with age from childhood through advancing age. The fiso lifespan trajectory also appears to be uncoupled from ficvf, echoing previous studies of white matter microstructural alterations over the course of the lifespan. These previous studies showed early and rapid increases in parenchymal neurite density in development (Lynch et al., 2020), followed by a slower decline with advancing age (Beck et al., 2021; Nazeri et al., 2015). It would be reasonable to assume that the free water volume fraction may be inversely correlated with ficvf, as increased myelination in development would reduce the extracellular space while neuronal atrophy in aging would increase the extracellular space. However, our findings demonstrating that the fiso lifespan trajectory in the parenchyma is uncoupled from the ficvf trajectory may reflect a more distinct process indicative of the important glymphatic process of bulk fluid flow. These findings are also independent of perivascular space diameter. Therefore, increased bulk fluid flow within and around PVS is not merely a by-product of the morphological enlargement of the spaces that contain freely diffusing fluid (Lynch et al., 2023). We also found fluid anisotropy increases in childhood and decreases in advancing age, due predominantly to the radial component of the tensor. Interestingly, these changes are accompanied by similar trends in the tissue tensor. Therefore, it is possible that the estimated fluid tensor is influenced by the microscopic boundaries of the surrounding parenchymal tissue.

Across free water diffusion metrics, we observed a ubiquitous trend wherein perivascular and parenchymal fluid content became more similar with age, due to faster changes in diffusion metrics in the parenchyma compared to the PVS. One possible interpretation for this trend toward sameness with age may be due to age-related breakdown of the blood-brain barrier and compromised PVS integrity due to reduced AQP4 channel polarization. These changes may result in the leakage of fluid between the PVS and surrounding parenchyma, thus resulting in more similar fluid signals with age.

We observed a reduction in free water anisotropy and volume in the brain parenchyma with distance from the PVS. Our findings suggest the amount and preferred direction of bulk flow is lowest in regions where enlarged PVS are not detected. Our findings are supported by a recent study in patients with cerebral small vessel disease (CSVD) and older subjects, where they observed a similar pattern of reduced fiso with distance from the PVS (Jiaerken et al., 2021). We found the rate of change in free water tensor metrics from the PVS to the periphery is greater in older subjects compared to developing children and adolescents, which may correspond to leakier PVS and less stable fluid homeostasis in aging. Aging is associated with reduced arterial pulsatility and disrupted blood-brain barrier permeability, which can alter interstitial fluid flow and further contribute to the pathogenesis of PVS dilation (Iliff et al., 2013).

To determine if age-related alterations in free water diffusion measures have functional consequences, we explored the interplay between age, diffusion metrics and gross cognitive performance. We observed an age-dependent relationship between fFA and cognitive performance in the developing cohort, but not the aging cohort, where the correlation between fFA and cognitive performance in both the parenchyma and PVS becomes increasingly negative with age. The relationship between global free diffusion properties in the brain and cognition may be more pronounced during adolescent development compared to aging due to the reduced incidence of confounding health effects that can influence cerebrovascular health and contribute to cognitive decline, such as CSVD (Hamilton et al., 2021; Tang et al., 2022) obesity (Nguyen et al., 2014; Raitamaa et al., 2024), and hypertension (Santisteban et al., 2023). However, in aging adults, we found a distance-dependent relationship between cognitive performance and the diffusion metrics fiso and fFA, where subjects with worse cognitive performance had a steeper rate of decrease in diffusion metrics in the parenchyma with distance from the PVS. Therefore, our results suggest free water diffusion measures exert a more subtle and localized influence on cognitive performance in aging subjects. The relationship between the structural components of the waste clearance system and cognition have been previously explored; however, evidence is mixed. Previous studies have shown the number of MR-visible PVS is associated with worse performance in global cognitive function (Libecap et al., 2022), information processing and executive function (Passiak et al., 2019). However, in a large meta-analysis, it was found that PVS counts were not associated with cognitive deficits in the general population (Hilal et al., 2018). However, this is the first study, to our knowledge, that interrogates this question using diffusion MRI measures of bulk fluid flow in both children and aging adults.

Our study explores the influence of diffusion MRI-derived measures of fluid flow properties in the PVS and parenchyma using large population-based datasets that cover the lifespan from development through advancing age. However, several limitations should be addressed. First, the present study is cross-sectional, and future studies should employ longitudinal designs to establish the relationship between fluid flow properties and changes in cognition. Additionally, while others have demonstrated the utility of using the NODDI model to probe the free water diffusion compartment as a measure of fluid flow properties, additional models derived from

ultra-low gradient strength diffusion MRI acquisitions, such as intra-voxel incoherent motion (IVIM), may provide improved sensitivity for bulk flow in the brain parenchyma (Wong et al., 2017, 2020). Together, further studies are needed to better understand the robustness of free water diffusion techniques in measuring fluid flow related to waste clearance.

Our findings demonstrate age-related alterations in free water diffusion metrics indicative of fluid flow properties in the perivascular space and surrounding parenchyma over the course of the lifespan. The results from this study suggest age-related PVS enlargement is accompanied by alterations in fluid exchange between the PVS and parenchyma and may indicate changing waste clearance functionality over the course of the life. Our findings also show perivascular and parenchymal fluid characteristics are predictive of cognitive outcomes during child development, where increased free water may lead to preferential impairments to cognition in older adolescents. Our findings therefore suggest altered fluid characteristics in the maturing brain may disrupt cognitive development, potentially due to inefficient waste clearance.

Competing Interest Statement

The perivascular space mapping technology is part of a pending patent owned by FS and JC, with no financial interest/conflict. JC declares status as employee of the private company NeuroScope Inc. (NY, USA)

Tables

Table 1. The influence of age, mean PVS diameter and sex on perivascular free water diffusion measures.

		Age			PVS diameter			Sex		
Measure	Cohort	*B*	Std Error	*t*	*B*	Std. Error	*t*	*B*	Std. Error	*t*
fiso	HCD	5.23×10^{-4}	1.65×10^{-4}	3.17**	0.0236	0.00207	11.329***	0.00413	0.00127	3.26*
	HCA	4.57×10^{-5}	5.06×10^{-5}	0.9	0.0205	0.0015	13.69***	0.00326	0.0013	2.51
ficvf	HCD	0.00589	3.22×10^{-4}	18.29***	-0.0256	0.00405	-6.34***	0.00639	0.00247	2.58
	HCA	-9.84×10^{-4}	1.14×10^{-4}	-8.60***	-0.0119	0.00339	-3.52***	0.00437	0.00294	1.49
fFA	HCD	0.00177	2.49×10^{-4}	7.10***	-0.0298	0.00313	-9.50***	0.0064	0.00192	3.34*
	HCA	-4.61×10^{-4}	5.75×10^{-5}	-8.01***	-0.0157	0.00169	-9.24***	0.00555	0.00148	3.76*
fAD	HCD	-4.41×10^{-7}	5.09×10^{-7}	-0.87	-1.63×10^{-5}	3.97×10^{-6}	-2.54*	1.68×10^{-5}	3.91×10^{-6}	4.31*
	HCA	-2.57×10^{-7}	1.11×10^{-7}	-2.32*	-1.03×10^{-6}	3.26×10^{-6}	-0.32	1.53×10^{-5}	2.84×10^{-5}	5.39*
fRD	HCD	-7.12×10^{-6}	1.06×10^{-6}	-6.70***	1.09×10^{-4}	1.34×10^{-5}	8.18***	-2.26×10^{-5}	8.16×10^{-6}	-2.76
	HCA	1.71×10^{-6}	2.07×10^{-7}	8.26***	5.90×10^{-5}	6.10×10^{-6}	9.68***	-1.78×10^{-5}	5.31×10^{-6}	-3.35*
fMD	HCD	-4.89×10^{-6}	7.06×10^{-7}	-6.93***	6.75×10^{-5}	8.87×10^{-6}	7.61***	-9.40×10^{-6}	5.42×10^{-6}	-1.7
	HCA	1.05×10^{-6}	1.32×10^{-7}	7.99***	3.90×10^{-5}	3.88×10^{-6}	10.04***	-6.78×10^{-6}	3.38×10^{-6}	-2.00

HCD – Development; HCA – Aging; *p<.05; **p<.01; ***<.001

Table 2. The influence of age, mean PVS diameter and sex on parenchymal free water diffusion measures.

		Age			PVS diameter			Sex		
Measure	Cohort	*B*	Std Error	*t*	*B*	Std. Error	*t*	*B*	Std. Error	*t*
fiso	HCD	0.00101	0.000109	9.26***	0.00808	0.00137	5.89***	0.00262	0.000837	3.14**
	HCA	1.51×10^{-4}	3.31×10^{-4}	4,56***	8.40×10^{-3}	9.81×10^{-4}	8.57***	0.00307	8.51×10^{-4}	3.61**,
ficvf	HCD	0.00624	0.00023	27.12***	-0.00583	0.0029	-2.01*	0.00264	0.00176	1.5
	HCA	-6.28×10^{-4}	8.62×10^{-5}	-7.29***	-0.00391	0.00256	-1.53	3.00387	0.00221	1.75
fFA	HCD	0.00194	0.000193	10.01***	-0.00331	0.00244	-1.36	0.00378	0.00149	2.53*
	HCA	-4.21×10^{-4}	5.14×10^{-5}	-8.20***	-0.00209	0.00152	1.38	0.00404	0.00132	3.06**
fAD	HCD	8.56×10^{-8}	5.15×10^{-7}	0.17	9.18×10^{-6}	6.48×10^{-6}	1.42	9.72×10^{-6}	3.96×10^{-6}	2.46*
	HCA	-7.79×10^{-8}	3.70×10^{-7}	-.211	1.51×10^{-5}	1.09×10^{-5}	1.39	2.14×10^{-5}	9.49×10^{-6}	2.26*
fRD	HCD	-7.16×10^{-6}	7.34×10^{-7}	-9.76***	1.65×10^{-5}	9.25×10^{-6}	1.78	-1.31×10^{-5}	5.64×10^{-6}	-2.32*
	HCA	1.69×10^{-6}	1.97×10^{-7}	8.57***	1.29×10^{-5}	5.81×10^{-6}	2.22*	-1.06×10^{-5}	5.06×10^{-6}	-2.10*
fMD	HCD	-4.74×10^{-6}	4.78×10^{-7}	-9.94***	1.40×10^{-5}	6.01×10^{-6}	2.33*	-5.48×10^{-6}	3.67×10^{-6}	-1.49
	HCA	1.10×10^{-6}	2.07×10^{-7}	5.30***	1.36×10^{-5}	6.12×10^{-6}	2.23*	2.83×10^{-8}	5.32×10^{-6}	0.005

HCD – Development; HCA – Aging; *p<.05; **p<.01; ***<.001

Table 3. The correlation between age and the PVS/parenchyma ratio of free water diffusion

Measure	Cohort	*r*	*p*
fiso	HCD	-0.348	<.0001
	HCA	-0.096	0.026
ficvf	HCD	-0.313	<.0001
	HCA	-0.444	<.0001
fFA	HCD	-0.091	0.054
	HCA	-0.167	0.0001
fAD	HCD	-0.061	0.191
	HCA	-0.051	0.24
fRD	HCD	0.045	0.347
	HCA	0.199	<.0001
fMD	HCD	-0.023	0.625
	HCA	0.09	0.038

HCD – Development; HCA – Aging

Table 4. The interaction between age and diffusion metrics on total cognition composite scores as assessed with the NIH Toolbox.

			metric		age		metric*age	
Cohort	Region	Metric	F	p	F	p	F	p
HCD	PVS	fFA	**13.19**	**0.0003**	**20.24**	**<.0001**	**15.54**	**<.0001**
		fiso	0.79	0.37	0.71	0.4	0.64	0.42
	Parenchyma	fFA	**12.07**	**0.0006**	**20.92**	**<.0001**	**16.7**	**<.0001**
		fiso	1.42	0.23	**11.82**	**0.0006**	2.77	0.09
HCA	PVS	fFA	0.2	0.66	0.06	0.81	0.01	0.94
		fiso	0.44	0.51	1.26	0.26	0.26	0.61
	Parenchyma	fFA	1.52	0.22	0.25	0.61	0.42	0.52
		fiso	0.53	0.47	0.74	0.39	0.09	0.76

HCD – Development; HCA – Aging

References

Andersson, J. L. R., & Sotiropoulos, S. N. (2016). An integrated approach to correction for off-resonance effects and subject movement in diffusion MR imaging. *NeuroImage*, *125*, 1063–1078. https://doi.org/10.1016/j.neuroimage.2015.10.019

Avants, B. B., Epstein, C. L., Grossman, M., & Gee, J. C. (2008). Symmetric diffeomorphic image registration with cross-correlation: Evaluating automated labeling of elderly and neurodegenerative brain. *Medical Image Analysis*, *12*(1), 26–41. https://doi.org/10.1016/j.media.2007.06.004

Banerjee, G., Kim, H. J., Fox, Z., Ja, H. R., Wilson, D., Charidimou, A., Na, H. K., Na, D. L., Seo, S. W., & Werring, D. J. (2017). MRI-visible perivascular space location is associated with Alzheimer' s disease independently of amyloid burden. *Brain*, *140*, 1107–1116. https://doi.org/10.1093/brain/awx003

Barisano, G., Lynch, K. M., Sibilia, F., Lan, H., Shih, N. C., Sepehrband, F., & Choupan, J. (2022). Imaging perivascular space structure and function using brain MRI. In *NeuroImage* (Vol. 257). Academic Press Inc. https://doi.org/10.1016/j.neuroimage.2022.119329

Beck, D., de Lange, A. M., Maximov, I. I., Richard, G., Andreassen, O. A., Nordvik, J. E., & Westlye, L. T. (2021). White matter microstructure across the adult lifespan: A mixed longitudinal and cross-sectional study using advanced diffusion models and brain-age prediction. *NeuroImage*, *224*. https://doi.org/10.1016/j.neuroimage.2020.117441

Bookheimer, S. Y., Salat, D. H., Terpstra, M., Ances, B. M., Barch, D. M., Buckner, R. L., Burgess, G. C., Curtiss, S. W., Diaz-Santos, M., Elam, J. S., Fischl, B., Greve, D. N., Hagy, H. A., Harms, M. P., Hatch, O. M., Hedden, T., Hodge, C., Japardi, K. C., Kuhn, T. P., … Yacoub, E. (2019). The Lifespan Human Connectome Project in Aging: An overview. *NeuroImage*, *185*(September 2018), 335–348. https://doi.org/10.1016/j.neuroimage.2018.10.009

Cabeen, R. P., Laidlaw, D. H., & Toga, A. W. (2018). Quantitative imaging toolkit: Software for interactive 3D visualization, data exploration, and computational analysis of neuroimaging datasets. *ISMRM-ESMRMB Abstracts*, 12–14.

Cabeen, R. P., Sepehrband, F., & Toga, A. W. (2019). Rapid and accurate NODDI parameter estimation with the spherical mean technique. *Proc International Society for Magnetic Resonance in Medicine (ISMRM)*, 3363.

Charidimou, A., Boulouis, G., Pasi, M., Etten, E. S. Van, Haley, K., Ayres, A., Schwab, K. M., & Greenberg, S. M. (2017). MRI-visible perivascular spaces in cerebral amyloid angiopathy and hypertensive arteriopathy. *American Academy of Neurology*, *88*, 1157–1164.

Charidimou, A., Meegahage, R., Fox, Z., Peeters, A., Vandermeeren, Y., Laloux, P., Baron, J. C., Jäger, H. R., & Werring, D. J. (2013). Enlarged perivascular spaces as a marker of underlying arteriopathy in intracerebral haemorrhage: A multicentre MRI cohort study. *Journal of Neurology, Neurosurgery and Psychiatry*, *84*(6), 624–629. https://doi.org/10.1136/jnnp-2012-304434

Debaker, C., Djemai, B., Ciobanu, L., Tsurugizawa, T., & Bihan, D. Le. (2020). Diffusion MRI reveals in vivo and non-invasively changes in astrocyte function induced by an aquaporin-4 inhibitor. *PLoS ONE*, *15*(5), 1–14. https://doi.org/10.1371/journal.pone.0229702

Dinov, I. D., van Horn, J. D., Lozev, K. M., Magsipoc, R., Petrosyan, P., Liu, Z., MacKenzie-Graham, A., Eggert, P., Parker, D. S., & Toga, A. W. (2009). Efficient, distributed and interactive neuroimaging data analysis using the LONI Pipeline. *Frontiers in Neuroinformatics*, *3*(JUL), 1–10. https://doi.org/10.3389/neuro.11.022.2009

Doubal, F. N., MacLullich, A. M. J., Ferguson, K. J., Dennis, M. S., & Wardlaw, J. M. (2010). Enlarged Perivascular Spaces on MRI Are a Feature of Cerebral Small Vessel Disease. *Stroke*, *41*(3), 450–454. https://doi.org/10.1161/STROKEAHA.109.564914

Frangi, A. F., Niessen, W. J., Vincken, K. L., & Viergever, M. A. (1998). Multiscale vessel enhancement filtering. *International Conference on Medical Image Computing and Computer-Assisted Intervention*, 130–137. https://doi.org/10.1007/BFb0056195

Glasser, M. F., Sotiropoulos, S. N., Wilson, J. A., Coalson, T. S., Fischl, B., Andersson, J. L., Xu, J., Jbabdi, S., Webster, M., Polimeni, J. R., van Essen, D. C., & Jenkinson, M. (2013). The minimal preprocessing pipelines for the Human Connectome Project. *NeuroImage*, *80*, 105–124. https://doi.org/10.1016/j.neuroimage.2013.04.127

Gomolka, R. S., Hablitz, L., Mestre, H., Giannetto, M., Du, T., Xie, L., Peng, W., Melero Martinez, P., Nedergaard, M., & Mori, Y. (2023). Loss of aquaporin-4 results in glymphatic system dysfunction via brain-wide interstitial fluid stagnation. *ELife*, *12*, e82232. https://doi.org/10.7554/eLife.82232

Greve, D., & Fischl, B. (2009). Accurate and robust brain image alignment using boundary-based registration. *Neuroimage*, *48*(1), 63–72.

Groeschel, S., Chong, W. K., Surtees, R., & Hanefeld, F. (2006). Virchow-Robin spaces on magnetic resonance images: normative data, their dilatation, and a review of the literature. *Neuroradiology*, *48*(10), 745–754. https://doi.org/10.1007/s00234-006-0112-1

Hamilton, O. K. L., Backhouse, E. V., Janssen, E., Jochems, A. C. C., Maher, C., Ritakari, T. E., Stevenson, A. J., Xia, L., Deary, I. J., & Wardlaw, J. M. (2021). Cognitive impairment in sporadic cerebral small vessel disease: A systematic review and meta-analysis. *Alzheimer's and Dementia*, *17*(4), 665–685. https://doi.org/10.1002/alz.12221

Harms, M., Somerville, L., Ances, B., Andersson, J., Barch, D., Bastiani, M., Bookheimer, S., Brown, T., Buckner, R., Burgess, G., Coalson, T., Chappell, M., Dapretto, M., Douaud, G., Fischl, B., Glasser, M., Greve, D., Hodge, C., Jamison, K., … Yacoub, E. (2018). Extending the Human Connectome Project across ages: Imaging protocols for the Lifespan Development and Aging projects. *Neuroimage*, *183*, 972–984.

Harrison, I. F., Siow, B., Akilo, A. B., Evans, P. G., Ismail, O., Ohene, Y., Nahavandi, P., Thomas, D. L., Lythgoe, M. F., & Wells, J. A. (2018). Non-invasive imaging of CSF-mediated brain clearance pathways via assessment of perivascular fluid movement with diffusion tensor MRI. *ELife*, *7*, 1–14. https://doi.org/10.7554/eLife.34028

Hilal, S., Tan, C. S., Adams, H. H. H., Habes, M., Mok, V., Venketasubramanian, N., Hofer, E., Kamran Ikram, M., Abrigo, J., Vernooij, M. W., Chen, C., Hosten, N., Volzke, H., Grabe, H. J., Schmidt, R., & Arfan Ikram, M. (2018). Enlarged perivascular spaces and cognition. *Neurology*, *91*(9), e832–e842. https://doi.org/10.1212/WNL.0000000000006079

Hoy, A. R., Koay, C. G., Kecskemeti, S. R., & Alexander, A. L. (2014). Optimization of a free water elimination two-compartment model for diffusion tensor imaging. *Neuroimaging*, *103*, 323–333. https://doi.org/10.1016/j.neuroimage.2014.09.053.Optimization

Iliff, J. J., Wang, M., Zeppenfeld, D. M., Venkataraman, A., Plog, B. A., Liao, Y., Deane, R., & Nedergaard, M. (2013). Cerebral arterial pulsation drives paravascular CSF–interstitial fluid exchange in the murine brain. *Journal of Neuroscience*, *33*(46), 18190–18199.

Jiaerken, Y., Lian, C., Huang, P., Yu, X., Zhang, R., Wang, S., Hong, H., Luo, X., Yap, P. T., Shen, D., & Zhang, M. (2021). Dilated perivascular space is related to reduced free-water in surrounding white matter among healthy adults and elderlies but not in patients with severe

cerebral small vessel disease. *Journal of Cerebral Blood Flow and Metabolism*. https://doi.org/10.1177/0271678X211005875

Keable, A., Fenna, K., Yuen, H. M., Johnston, D. A., Smyth, N. R., Smith, C., Salman, R. A. S., Samarasekera, N., Nicoll, J. A. R., Attems, J., Kalaria, R. N., Weller, R. O., & Carare, R. O. (2016). Deposition of amyloid β in the walls of human leptomeningeal arteries in relation to perivascular drainage pathways in cerebral amyloid angiopathy. *Biochimica et Biophysica Acta - Molecular Basis of Disease*, *1862*(5), 1037–1046. https://doi.org/10.1016/j.bbadis.2015.08.024

Kilsdonk, I. D., Steenwijk, M. D., Pouwels, P. J. W., Zwanenburg, J. J. M., Visser, F., Luijten, P. R., Geurts, J. J. G., Barkhof, F., & Wattjes, M. P. (2015). Perivascular spaces in MS patients at 7 Tesla MRI: A marker of neurodegeneration? *Multiple Sclerosis Journal*, *21*(2), 155–162. https://doi.org/10.1177/1352458514540358

Libecap, T. J., Zachariou, V., Bauer, C. E., Wilcock, D. M., Jicha, G. A., Raslau, F. D., & Gold, B. T. (2022). Enlarged Perivascular Spaces Are Negatively Associated With Montreal Cognitive Assessment Scores in Older Adults. *Frontiers in Neurology*, *13*. https://doi.org/10.3389/fneur.2022.888511

Lynch, K. M., Cabeen, R. P., Toga, A. W., & Clark, K. A. (2020). Magnitude and timing of major white matter tract maturation from infancy through adolescence with NODDI. *NeuroImage*, *212*, 4–7. https://doi.org/10.1016/j.neuroimage.2020.116672

Lynch, K. M., Sepehrband, F., Toga, A. W., & Choupan, J. (2023). Brain perivascular space imaging across the human lifespan. *NeuroImage*, *271*. https://doi.org/10.1016/j.neuroimage.2023.120009

Nazeri, a., Chakravarty, M. M., Rotenberg, D. J., Rajji, T. K., Rathi, Y., Michailovich, O. V., & Voineskos, a. N. (2015). Functional Consequences of Neurite Orientation Dispersion and Density in Humans across the Adult Lifespan. *Journal of Neuroscience*, *35*(4), 1753–1762. https://doi.org/10.1523/JNEUROSCI.3979-14.2015

Nguyen, J. C. D., Killcross, A. S., & Jenkins, T. A. (2014). Obesity and cognitive decline: Role of inflammation and vascular changes. *Frontiers in Neuroscience*, *8*(OCT). https://doi.org/10.3389/fnins.2014.00375

Okar, S. V., Hu, F., Shinohara, R. T., Beck, E. S., Reich, D. S., & Ineichen, B. V. (2023). The etiology and evolution of magnetic resonance imaging-visible perivascular spaces: Systematic review and meta-analysis. In *Frontiers in Neuroscience* (Vol. 17). Frontiers Media SA. https://doi.org/10.3389/fnins.2023.1038011

Passiak, B. S., Liu, D., Kresge, H. A., Cambronero, F. E., Pechman, K. R., Osborn, K. E., Gifford, K. A., Hohman, T. J., Schrag, M. S., Davis, L. T., & Jefferson, A. L. (2019). Perivascular spaces contribute to cognition beyond other small vessel disease markers. *Neurology*, *92*(12), E1309–E1321. https://doi.org/10.1212/WNL.0000000000007124

Pasternak, O., Sochen, N., Gur, Y., Intrator, N., & Assaf, Y. (2009). Free water elimination and mapping from diffusion MRI. *Magnetic Resonance in Medicine*, *62*(3), 717–730. https://doi.org/10.1002/mrm.22055

Potter, G. M., Doubal, F. N., Jackson, C. A., Chappell, F. M., Sudlow, C. L., Dennis, M. S., & Wardlaw, J. M. (2015). Enlarged perivascular spaces and cerebral small vessel disease. *International Journal of Stroke*, *10*(3), 376–381. https://doi.org/10.1111/ijs.12054

Poulain, A., Riseth, J., & Vinje, V. (2023). Multi-compartmental model of glymphatic clearance of solutes in brain tissue. *PLOS ONE*, *18*(3), e0280501. https://doi.org/10.1371/journal.pone.0280501

Raitamaa, L., Kautto, J., Tuunanen, J., Helakari, H., Huotari, N., Järvelä, M., Korhonen, V., & Kiviniemi, V. (2024). Association of body-mass index with physiological brain pulsations across adulthood – a fast fMRI study. *International Journal of Obesity*. https://doi.org/10.1038/s41366-024-01515-5

Reuter, M., Rosas, H. D., & Fischl, B. (2010). Highly Accurate Inverse Consistent Registration: A Robust Approach. *NeuroImage*, *53*(4), 1181–1196. https://doi.org/10.1016/j.neuroimage.2010.07.020

Santisteban, M. M., Iadecola, C., & Carnevale, D. (2023). Hypertension, Neurovascular Dysfunction, and Cognitive Impairment. In *Hypertension* (Vol. 80, Issue 1, pp. 22–34). Lippincott Williams and Wilkins. https://doi.org/10.1161/HYPERTENSIONAHA.122.18085

Segonne, F., Dale, A. M., Busa, E., Glessner, M., Salat, D., Hahn, H. K., & Fischl, B. (2004). A hybrid approach to the skull stripping problem in MRI. *NeuroImage*, *22*(3), 1060–1075. https://doi.org/DOI: 10.1016/j.neuroimage.2004.03.032

Sepehrband, F., Barisano, G., Sheikh-Bahaei, N., Cabeen, R. P., Choupan, J., Law, M., & Toga, A. W. (2019). Image processing approaches to enhance perivascular space visibility and quantification using MRI. *Scientific Reports*, *9*, 12351. https://doi.org/https://doi.org/10.1038/s41598-019-48910-x

Sepehrband, F., Barisano, G., Sheikh-Bahaei, N., Choupan, J., Cabeen, R. P., Lynch, K. M., Crawford, M. S., Lan, H., Mack, W. J., Chui, H. C., Ringman, J. M., & Toga, A. W. (2021). Volumetric distribution of perivascular space in relation to mild cognitive impairment. *Neurobiology of Aging*, *99*, 28–43. https://doi.org/10.1016/j.neurobiolaging.2020.12.010

Sepehrband, F., Cabeen, R. P., Barisano, G., Sheikh-Bahaei, N., Choupan, J., Law, M., & Toga, A. W. (2019). Nonparenchymal fluid is the source of increased mean diffusivity in preclinical Alzheimer's disease. *Alzheimer's & Dementia: Diagnosis, Assessment & Disease Monitoring*, *11*, 348–354. https://doi.org/10.1016/j.dadm.2019.03.002

Sepehrband, F., Cabeen, R. P., Choupan, J., Barisano, G., Law, M., & Toga, A. W. (2019). Perivascular space fluid contributes to diffusion tensor imaging changes in white matter. *Neuroimage*, *197*, 243–254. https://doi.org/10.1016/j.neuroimage.2019.04.070

Sled, J. G., Zijdenbos, A. P., & Evans, A. C. (1998). A nonparametric method for automatic correction of intensity nonuniformity in MRI data. *IEEE Transactions on Medical Imaging*, *17*(1), 87–97. https://doi.org/10.1109/42.668698

Somerville, L. H., Bookheimer, S. Y., Buckner, R. L., Burgess, G. C., Curtiss, S. W., Dapretto, M., Elam, J. S., Gaffrey, M. S., Harms, M. P., Hodge, C., Kandala, S., Kastman, E. K., Nichols, T. E., Schlaggar, B. L., Smith, S. M., Thomas, K. M., Yacoub, E., Van Essen, D. C., & Barch, D. M. (2018). The Lifespan Human Connectome Project in Development: A large-scale study of brain connectivity development in 5–21 year olds. *NeuroImage*, *183*(August), 456–468. https://doi.org/10.1016/j.neuroimage.2018.08.050

Sotiropoulos, S. N., Jbabdi, S., Xu, J., Andersson, J. L., Moeller, S., Auerbach, E. J., Glasser, M. F., Hernandez, M., Sapiro, G., Jenkinson, M., Feinberg, D. A., Yacoub, E., Lenglet, C., van Essen, D. C., Ugurbil, K., & Behrens, T. E. J. (2013). Advances in diffusion MRI acquisition and processing in the Human Connectome Project. *NeuroImage*, *80*, 125–143. https://doi.org/10.1016/j.neuroimage.2013.05.057

Sun, Z., Li, C., Wisniewski, T. W., Haacke, E. M., & Ge, Y. (2024). In Vivo Detection of Age-Related Tortuous Cerebral Small Vessels using Ferumoxytol-enhanced 7T MRI. *Aging and Disease*. https://doi.org/10.14336/AD.2023.1110-1

Tang, J., Zhang, M., Liu, N., Xue, Y., Ren, X., Huang, Q., Shi, L., & Fu, J. (2022). The Association Between Glymphatic System Dysfunction and Cognitive Impairment in Cerebral Small Vessel Disease. *Frontiers in Aging Neuroscience*, *14*. https://doi.org/10.3389/fnagi.2022.916633

Wardlaw, J. M., Smith, C., & Dichgans, M. (2013). Mechanisms of sporadic cerebral small vessel disease: Insights from neuroimaging. In *The Lancet Neurology* (Vol. 12, Issue 5, pp. 483–497). https://doi.org/10.1016/S1474-4422(13)70060-7

Wong, S. M., Backes, W. H., Drenthen, G. S., Zhang, C. E., Voorter, P. H. M., Staals, J., van Oostenbrugge, R. J., & Jansen, J. F. A. (2020). Spectral Diffusion Analysis of Intravoxel Incoherent Motion MRI in Cerebral Small Vessel Disease. *Journal of Magnetic Resonance Imaging*, *51*(4), 1170–1180. https://doi.org/10.1002/jmri.26920

Wong, S. M., Zhang, C. E., van Bussel, F. C. G., Staals, J., Jeukens, C. R. L. P. N., Hofman, P. A. M., van Oostenbrugge, R. J., Backes, W. H., & Jansen, J. F. A. (2017). Simultaneous investigation of microvasculature and parenchyma in cerebral small vessel disease using intravoxel incoherent motion imaging. *NeuroImage: Clinical*, *14*, 216–221. https://doi.org/10.1016/j.nicl.2017.01.017

Xue, Y., Liu, N., Zhang, M., Ren, X., Tang, J., & Fu, J. (2020). Concomitant enlargement of perivascular spaces and decrease in glymphatic transport in an animal model of cerebral small vessel disease. *Brain Research Bulletin*, *161*(March), 78–83. https://doi.org/10.1016/j.brainresbull.2020.04.008

Zhang, H., Schneider, T., Wheeler-Kingshott, C. A., & Alexander, D. C. (2012). NODDI: practical in vivo neurite orientation dispersion and density imaging of the human brain. *NeuroImage*, *61*(4), 1000–1016. https://doi.org/10.1016/j.neuroimage.2012.03.072

Zong, X., Lian, C., Jimenez, J., Yamashita, K., Shen, D., & Lin, W. (2020). Morphology of perivascular spaces and enclosed blood vessels in young to middle-aged healthy adults at 7T: Dependences on age, brain region, and breathing gas. *NeuroImage*, *218*(May), 116978. https://doi.org/10.1016/j.neuroimage.2020.116978

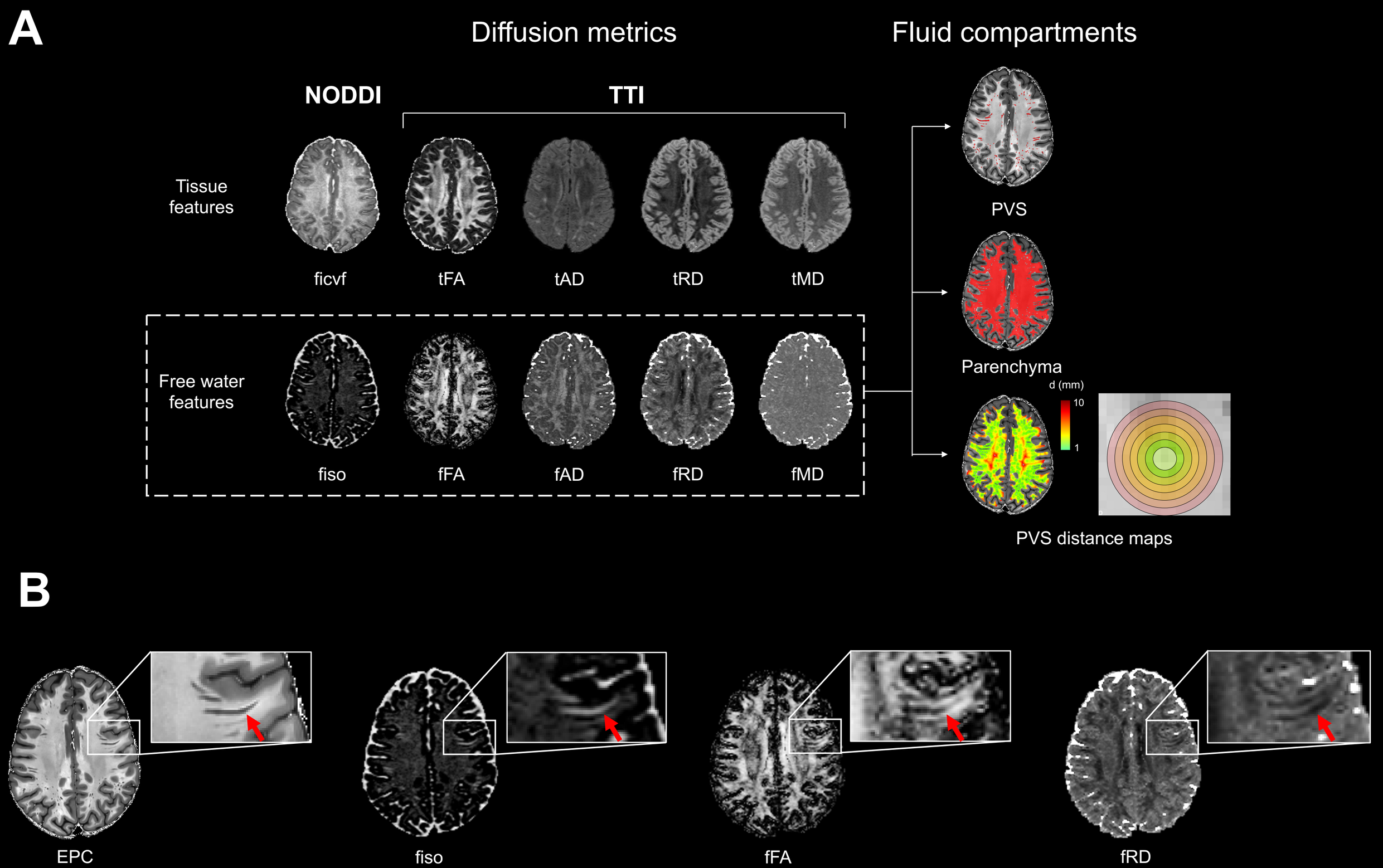
A
Diffusion metrics
Fluid compartments
NODDI
TTI
Tissue features
ficvf
tFA
tAD
tRD
tMD
Free water features
fiso
fFA
fAD
fRD
fMD
PVS
Parenchyma
d (mm)
10
1
PVS distance maps
B
EPC
fiso
fFA
fRD

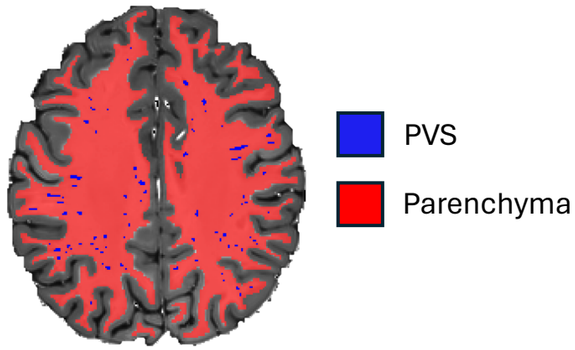
PVS
Parenchyma

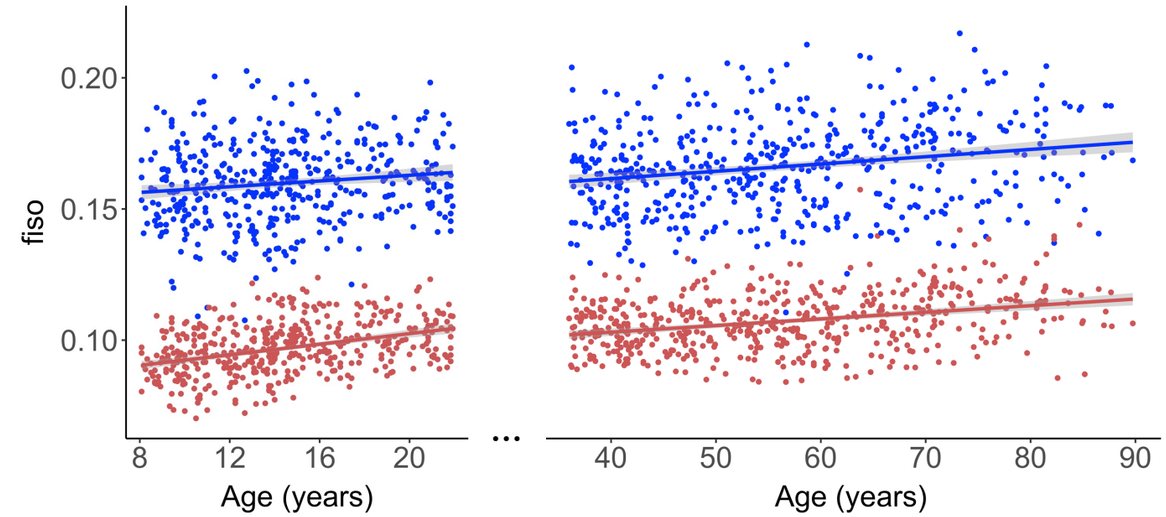
fiso
0.20
0.15
0.10
8
12
16
20
...
40
50
60
70
80
90
Age (years)
Age (years)

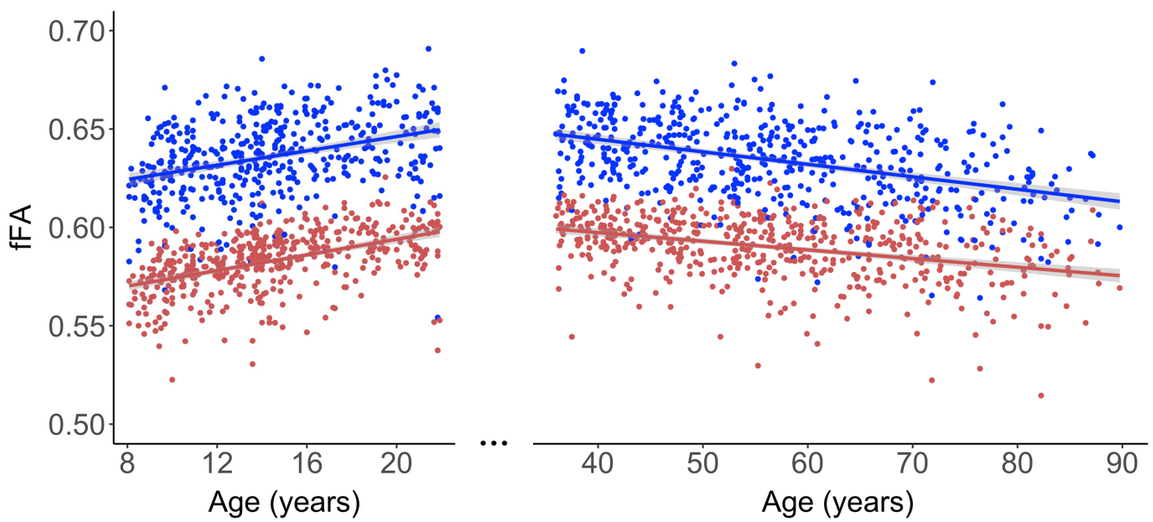
fFA
0.70
0.65
0.60
0.55
0.50
8
12
16
20
...
40
50
60
70
80
90
Age (years)
Age (years)

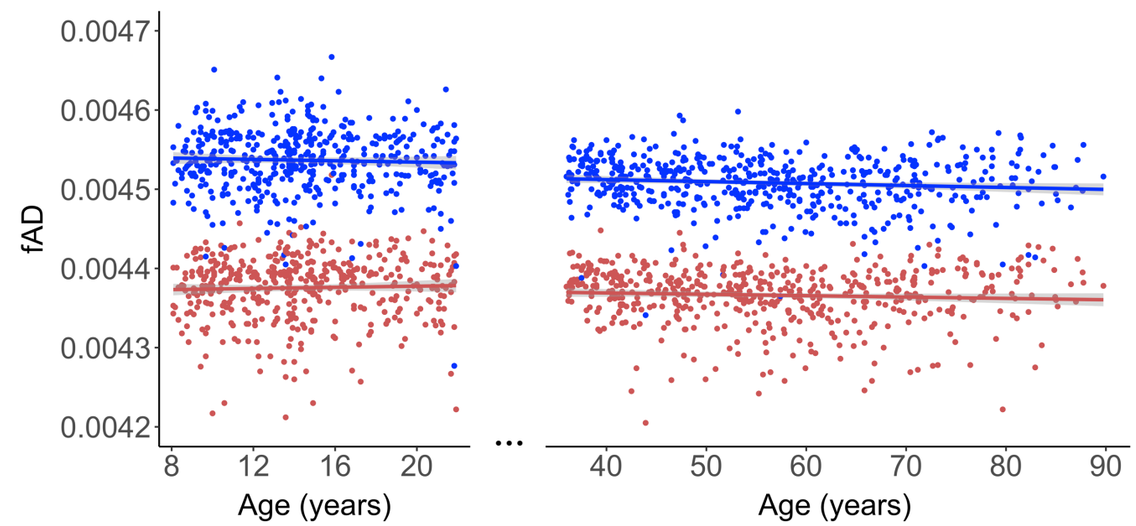
fAD
0.0047
0.0046
0.0045
0.0044
0.0043
0.0042
8
12
16
20
...
40
50
60
70
80
90
Age (years)
Age (years)

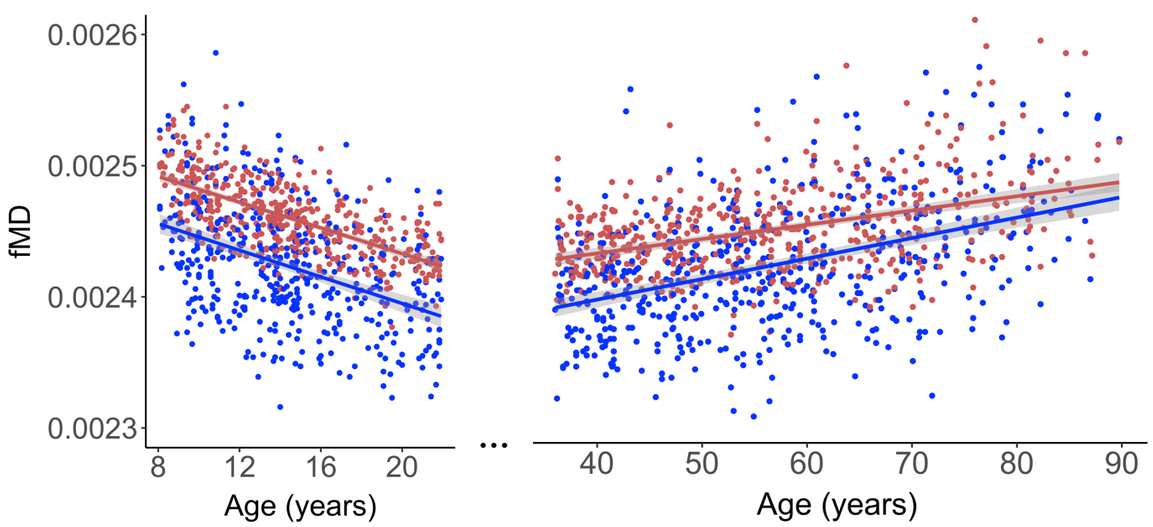
fMD
0.0026
0.0025
0.0024
0.0023
8
12
16
20
...
40
50
60
70
80
90
Age (years)
Age (years)

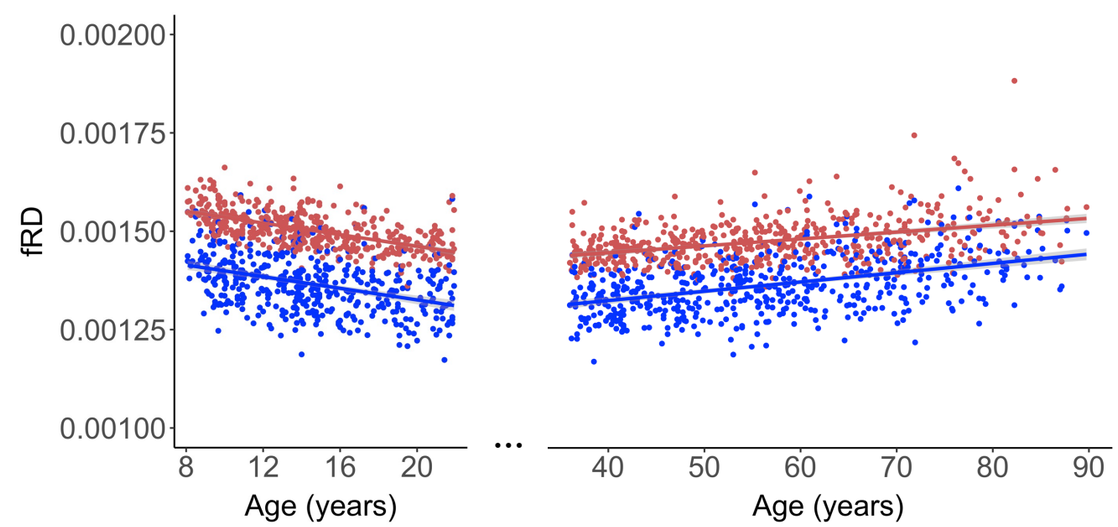
fRD
0.00200
0.00175
0.00150
0.00125
0.00100
8
12
16
20
...
40
50
60
70
80
90
Age (years)
Age (years)

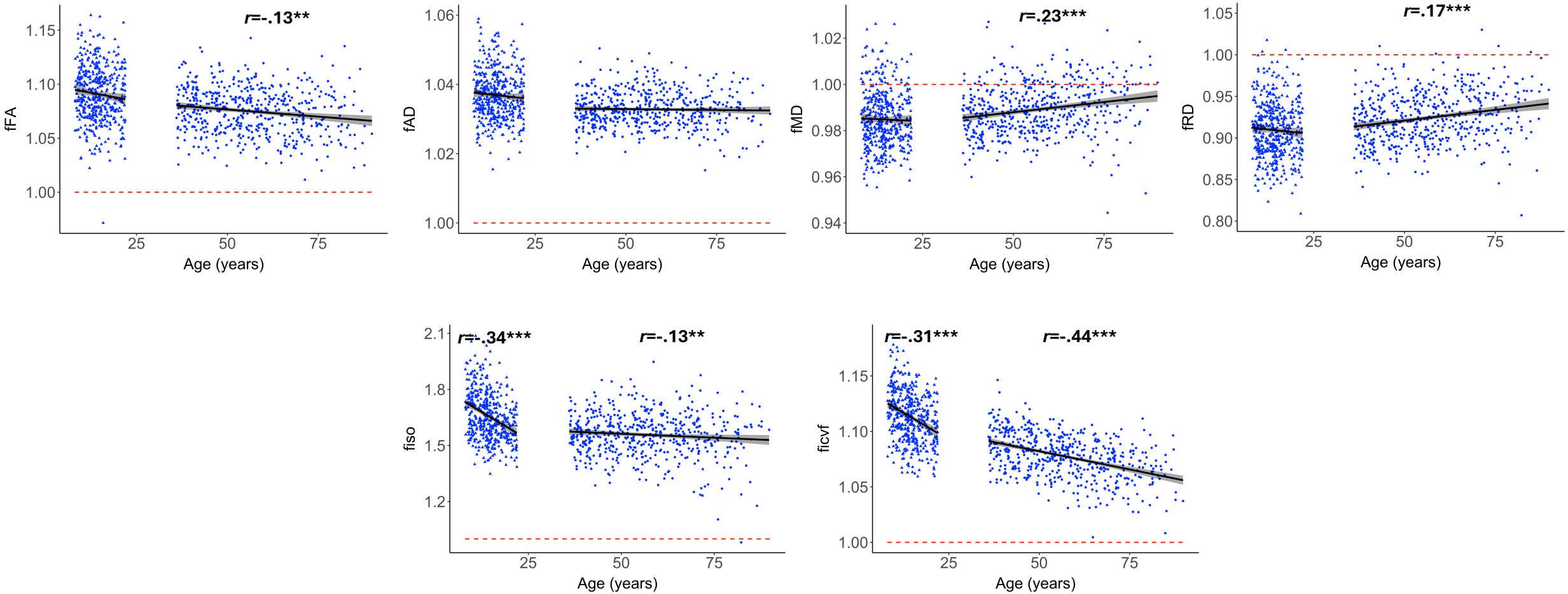
r=-.13**
fFA
1.15
1.10
1.05
1.00
25
50
75
Age (years)
fAD
1.06
1.04
1.02
1.00
r=.23***
fMD
1.02
1.00
0.98
0.96
0.94
r=.17***
fRD
1.05
1.00
0.95
0.90
0.85
0.80
r=-.34***
r=-.13**
fiso
2.1
1.8
1.5
1.2
r=-.31***
r=-.44***
ficvf

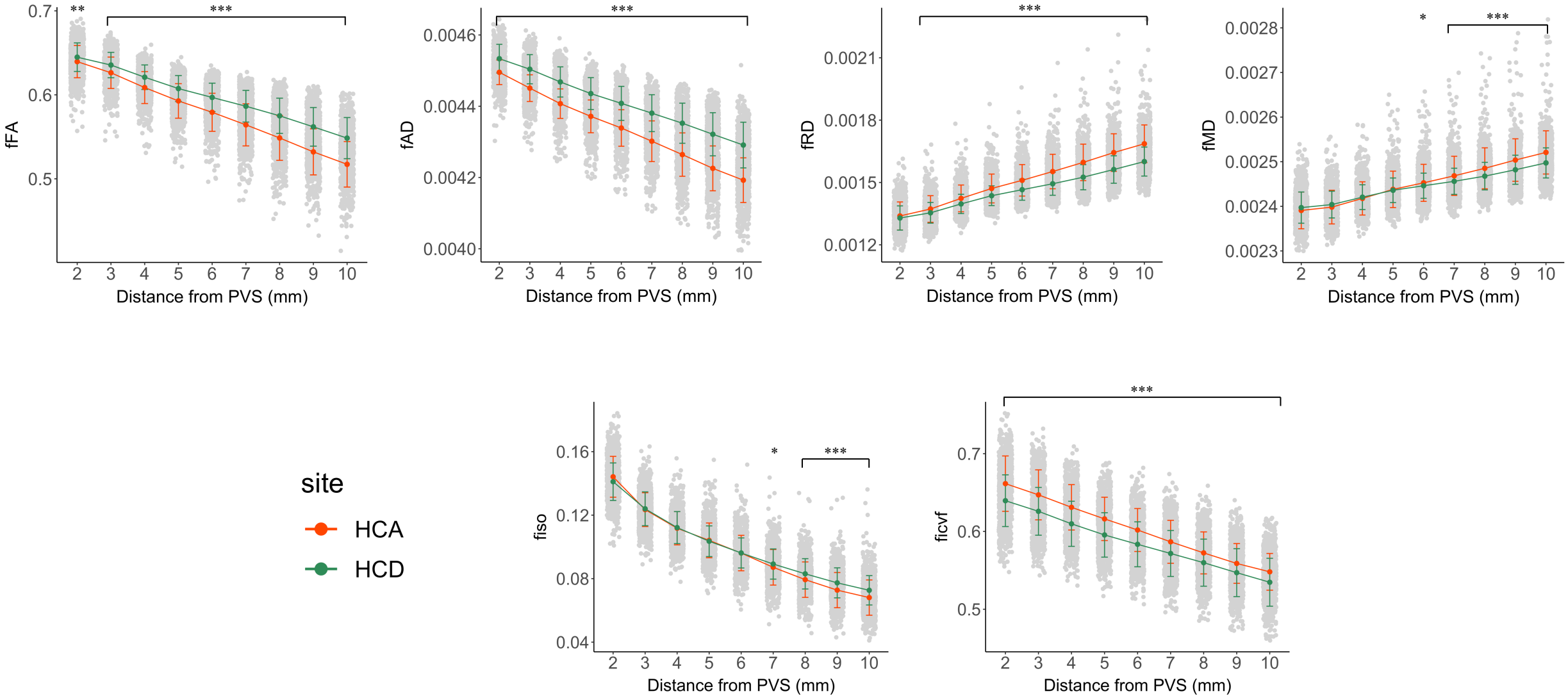
fFA
fAD
fRD
fMD
fiso
ficvf
Distance from PVS (mm)
site
HCA
HCD
*
**
***

A. PVS

HCP Development (8-21 years)

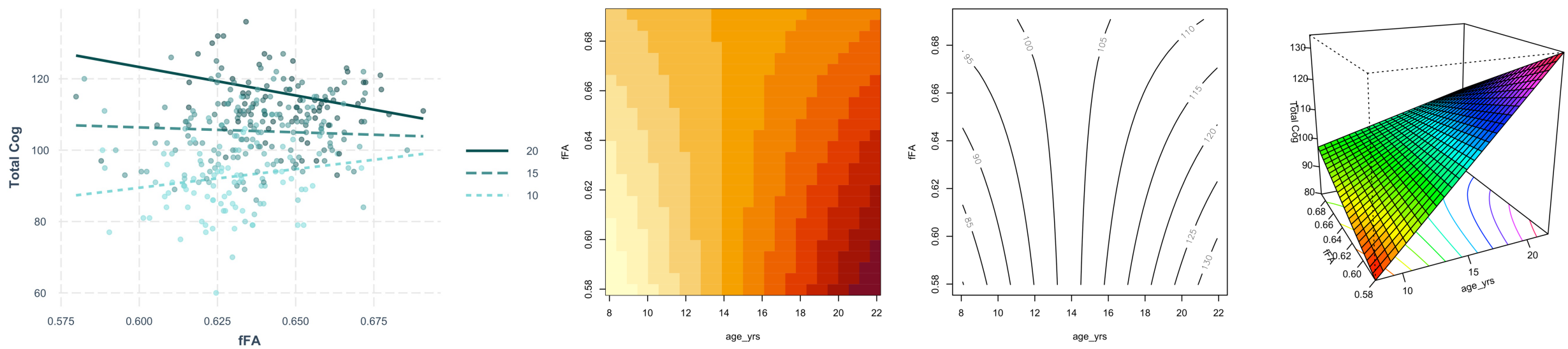

HCP Aging (35-90 years)

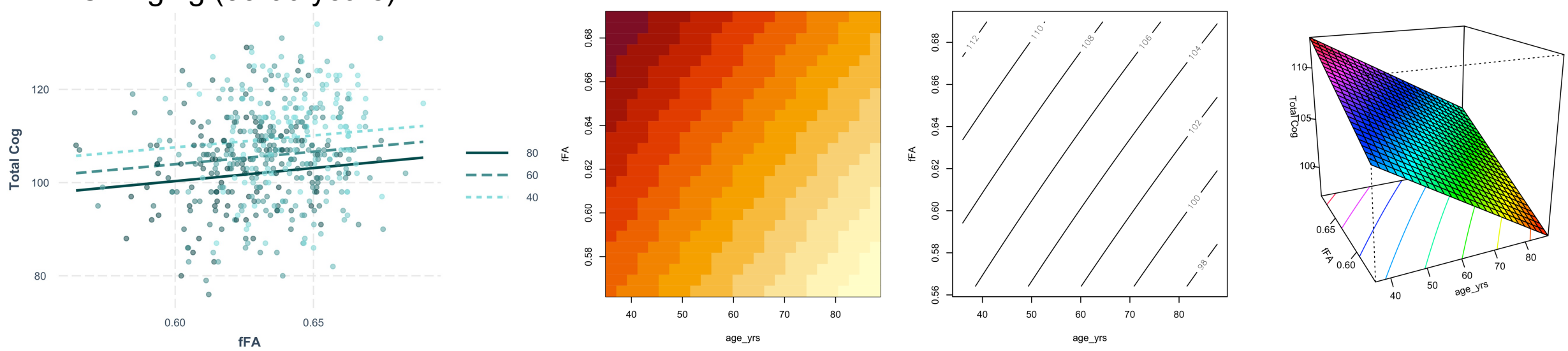

B. Parenchyma

HCP Development (8-21 years)

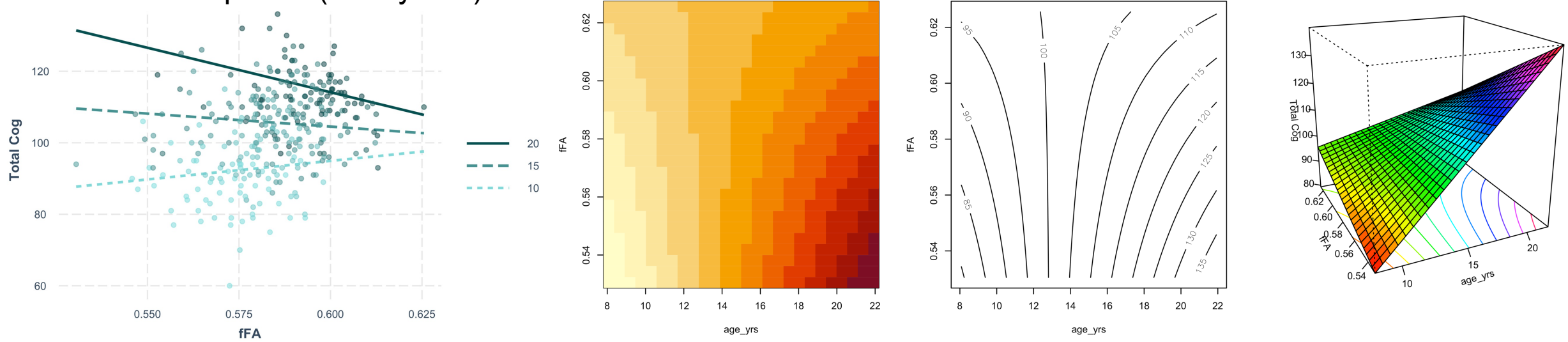

HCP Aging (35-90 years)

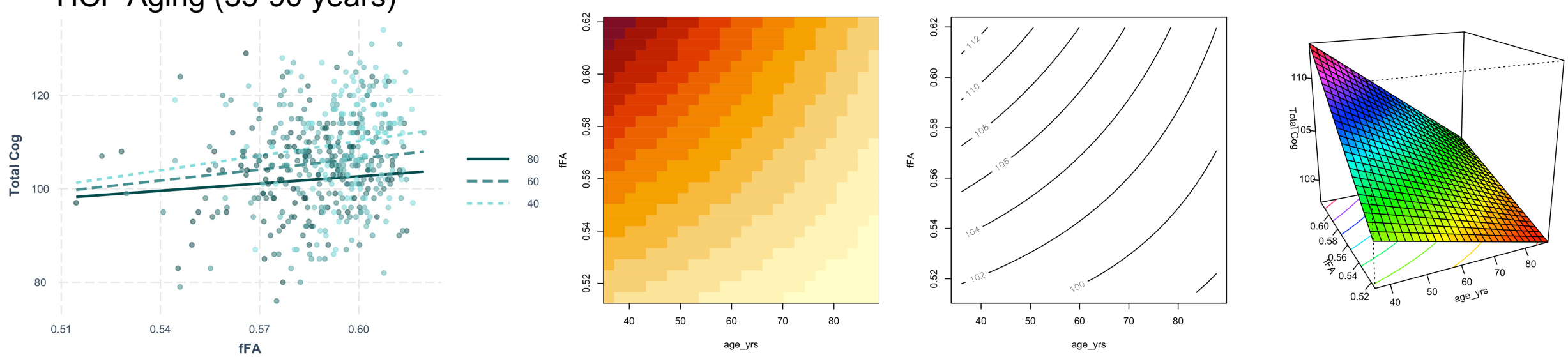

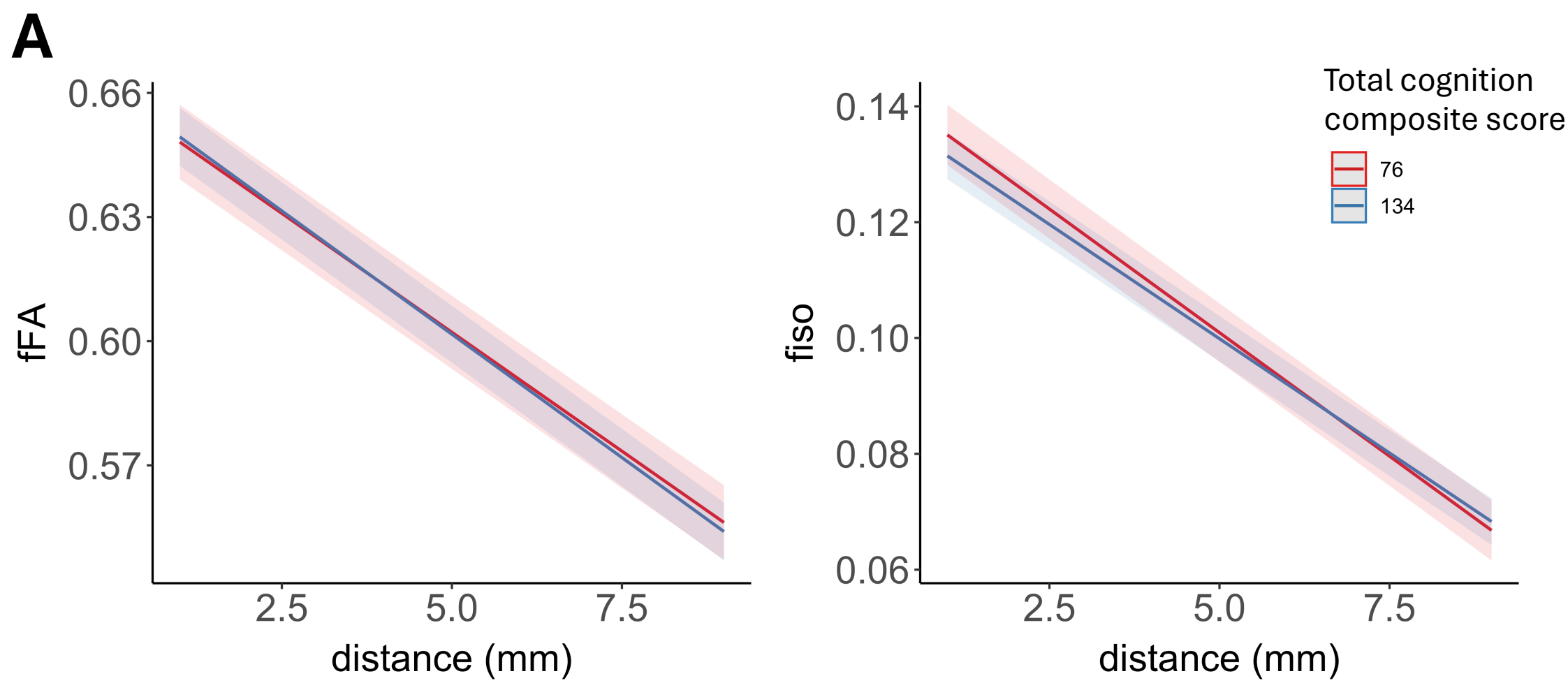
A
0.66
0.63
0.60
0.57
fFA
2.5
5.0
7.5
distance (mm)
0.14
0.12
0.10
0.08
0.06
fiso
2.5
5.0
7.5
distance (mm)
Total cognition
composite score
76
134

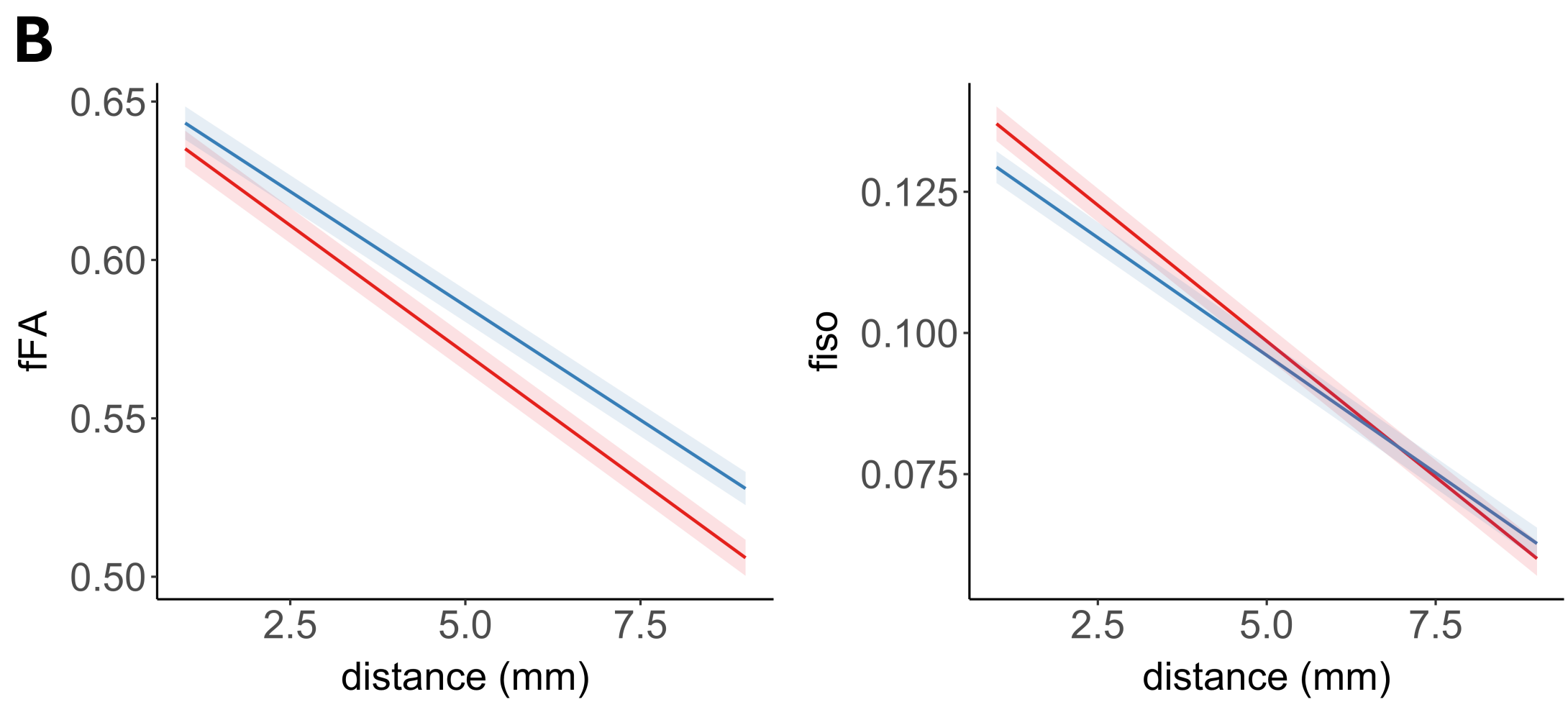
B
0.65
0.60
0.55
0.50
fFA
2.5
5.0
7.5
distance (mm)
0.125
0.100
0.075
fiso
2.5
5.0
7.5
distance (mm)